PHYSICAL REVIEW D **94,** 055003 (2016)

Flavor violating signatures of lighter and heavier Higgs bosons within the two Higgs doublet model type III at the LHeC

S. P. Das[*]

Instituto de Física, Benemérita Universidad Autónoma de Puebla, Apdo. Postal J-48, C.P. 72570 Puebla, Puebla, México and Facultad de Ciencias Físico-Matemáticas, Benemérita Universidad Autónoma de Puebla, Apdo. Postal 1364, C.P. 72570 Puebla, Puebla, México

J. Hernández-Sánchez[†]

Facultad de Ciencias de la Electrónica, Benemérita Universidad Autónoma de Puebla, Apdo. Postal 542, C.P. 72570 Puebla, Puebla, México and Dual C-P Institute of High Energy Physics, México

S. Moretti[‡]

School of Physics and Astronomy, University of Southampton, Highfield, Southampton SO17 1BJ, United Kingdom, and Particle Physics Department, Rutherford Appleton Laboratory, Chilton, Didcot, Oxon OX11 0QX, United Kingdom

A. Rosado[§]

Instituto de Física, Benemérita Universidad Autónoma de Puebla, Apdo. Postal J-48, C.P. 72570 Puebla, Puebla, México

R. Xoxocotzi[¶]

Facultad de Ciencias Físico-Matemáticas, Benemérita Universidad Autónoma de Puebla, Apdo. Postal 1364, C.P. 72570 Puebla, Puebla, México

(Received 9 May 2016; published 6 September 2016)

We analyze the prospects for observing the light and heavy CP-even neutral Higgs bosons ($\phi = h$ and H) in their decays into flavor violating $b\bar{s}$ channels (including charge conjugation) at the proposed Large Hadron electron Collider (LHeC), with $\sqrt{s} \approx 1.3$ TeV, in the framework of a 2-Higgs doublet model (2HDM) Type III, assuming a four-zero texture in the Yukawa matrices and a general Higgs potential. We consider theoretically consistent scenarios in agreement with current experimental data from flavor and Higgs physics. We investigate the charged current production process $\nu_e \phi q$ in presence of flavor violating decays of the Higgs bosons, that lead to a 3-jets + $\not{E}_T$ signature. We demand exactly two jets, one tagged b-jet and one light-flavor jet, all in the central rapidity region. The remaining jet (originated by the remnant quark q) is tagged in the forward or backward regions and this together with a central jet veto (not more than one light-flavor jet) are essential criterions to enhance the signal–to–background rates. We consider the most relevant standard model (SM) backgrounds, treating c-jets separately from light-flavor and gluon ones, while allowing for mistagging. We find that the SM-like Higgs boson, h, would be accessible within several parameter configurations of our model at approximately the 1-2σ level with 100 fb^{-1} of data. We also find that the heaviest neutral Higgs boson, H, with mass up to 150 GeV, would have a 1σ significance for the same data sample. At the end of the LHeC running, one would have ten times data accumulation and for all the Higgs masses the significances are enhanced so as to allow for detection of both the h and H state. Hence, one of the most viable extensions of 2HDMs with flavor changing neutral currents (FCNCs) generated at tree level but controlled by a four-zero texture approach in the Yukawa matrices, as opposed to the adoption of *ad hoc* discrete symmetries, could be put under scrutiny at a future ep machine.

DOI: 10.1103/PhysRevD.94.055003

I. INTRODUCTION

The standard model (SM) is well established by now after the discovery of a Higgs boson by the ATLAS [1] and CMS [2] experiments at the Large Hadron Collider (LHC). However, when one considers some theoretical aspects of

[*]sprasad@ifuap.buap.mx
[†]jaime.hernandez@correo.buap.mx
[‡]s.moretti@soton.ac.uk
[§]rosado@ifuap.buap.mx
[¶]xoxo_reyna@yahoo.com.mx

the SM, for example, lepton number violation, which is already manifested in the form of small but nonzero neutrino masses and actively searched for in the other two fermionic sectors [e.g., in $\mu \to e\gamma$ decays by the MEG experiment [3] and in B-physics by *BABAR* [4–7] and Belle [8–10],[1] one necessarily has to postulate new physics (NP) Beyond the SM (BSM)]. By combining the evidence of Higgs states and the presence in Nature of flavor violation, then one is well motivated in searching for evidence of BSM physics in a context where the two aspects merge, i.e., in flavor violating Higgs boson decays. In general, limited to the Higgs sector, several BSM scenarios have been invoked by introducing extra Higgs singlets, doublets and/or triplets. As the Higgs boson discovery at the LHC is consistent with a doublet structure, we refrain here from considering BSM constructions with either of the other two aforementioned Higgs representations. Therefore, in staying with multi-Higgs doublet structures, the simplest of such Higgs scenarios is the so called 2-Higgs doublet model (2HDM) [11,12], which will be the theoretical focus of our study. Other frameworks of the 2HDM supress FCNCs, which have been studied and they give rise to a variety of specific implementations [13–16].

Among the many phenomenological sides of a 2HDM, we are indeed concerned here with flavor violating Higgs boson decays in the quark sector, building on previous works of ours, see, e.g., Refs. [17–25]. However, plentiful of studies, also including lepton flavor violating scenarios, exist, some specific to 2HDMs and others adaptable to their case: see for an incomplete list, e.g., Refs. [26–51].

The actual search scope for Higgs bosons in flavor violating modes at the LHC has also been actively studied, see [52–59].[2] It has also been investigated in the context of a future e^+e^- [62] and $\gamma\gamma$ collider [22]. Prospects at a future hadron collider have been investigated in [57].

Herein, we are particularly motivated by a possible enhancement of flavor violating quark decays ($\phi \to b\bar{s}$) of intermediate mass Higgs bosons (below the top-quark mass) and we will focus on the possibility to access such signatures at the possibly upcoming Large Hadron electron Collider (LHeC). The LHeC facility [63] presently discussed as possible at CERN in the near future would be a Deep Inelastic Scattering (DIS) experiment at the TeV scale, with center-of-mass energy of around 1.3 TeV. In comparison to the another recently closed (in 2007) DIS experiment (the Hadron-Electron Ring Accelerator (HERA) [64] at DESY of around 320 GeV in energy with integrated luminosity of around 0.5 fb^{-1}), the LHeC might deliver data samples of approximately 100 fb^{-1} and with a higher detector coverage. Further, the overall kinematic range (in x and Q^2) accessible at LHeC is 20 times larger than at HERA.

While the primary task of a collider like the LHeC will be in-depth studies of QCD, the machine also affords some scope to study Higgs bosons decaying via flavor violating processes [65]. Our objective in this paper is to study the feasibility of finding two CP-even neutral Higgs bosons, the SM-like Higgs state h and its heavier counterpart H, at the upcoming LHeC assuming as BSM framework a 2HDM Type-III (henceforth 2HDM-III for short), which embodies a four-zero texture approach in the Yukawa matrices as the mechanism to control flavor changing neutral currents (FCNCs). As we have shown in previous analyses, this is precisely the framework which establishes $\phi \to b\bar{s} + \text{c.c.}$ as a hallmark signature of quark flavor violation in the Higgs sector whose detectability is under investigation at the LHC and future e^+e^- and $\gamma\gamma$ collider. However, we think ep experiments are the most appropriate in order to look for quark violating effects, because, even if it is possible to reach more energy in pp experiments, the surroundings to the latter processes are not cleaner than the former ones. The advantage of the ep collider kinematics comes from the possibility to disentangle the direction of the struck parton and the outgoing lepton. Further, an ep collider lacks the complications due to the backgrounds in comparison con pp-collider. Conversely, the experiments at e^-e^+-colliders will be cleaner than those at e^-p colliders, but the latter will provide more energetic collisions than the former [66,67]. Therefore, we can expect that all such machines will be competitive.

The plan of our paper is as follows. In the next section we describe briefly the theoretical structure of the 2HDM-III with a four-zero texture embedded in the Yukawa matrices. In Sec. III, we demarcate the allowed 2HDM-III parameter space in presence of both theoretical and experimental constraints. In Sec. IV, we explain the characteristics of the Higgs boson signal from charged current production. We introduce the most important SM backgrounds and finally, we carry out both a parameter space scan and a signal-to-backgrounds analysis for some characteristic benchmarks by adopting a simple cut-based optimization to isolate $\phi \to b\bar{s} + \text{c.c.}$ events. In Sec. V, we recap and present our conclusions.

II. THE HIGGS-YUKAWA SECTOR OF THE 2HDM TYPE-III

In the 2HDM, the two Higgs scalar doublets, $\Phi_1^\dagger = (\phi_1^-, \phi_1^{0*})$ and $\Phi_2^\dagger = (\phi_2^-, \phi_2^{0*})$, have the same hypercharge $+1$ such that both couple to the same quark flavor. Since a specific four-zero texture is implemented as a flavor symmetry in the Yukawa sector, this is the mechanism which controls FCNCs so that discrete symmetries in the Higgs potential are not needed [18,20,22]. Then the most

[1]In fact, also top-quark flavor violating decays into charm quarks and Higgs bosons are currently under investigation at the LHC.

[2]Current experimental results at the LHC include both ATLAS [60] and CMS [61] analyses.

general $SU(2)_L \times U(1)_Y$ invariant scalar potential, following [12], can be written as:

$$
\begin{aligned}
&V(\Phi_1,\Phi_2)\\
&\quad=\mu_1^2(\Phi_1^\dagger\Phi_1)+\mu_2^2(\Phi_2^\dagger\Phi_2)-(\mu_{12}^2(\Phi_1^\dagger\Phi_2)+\text{H.c.})\\
&\qquad+\frac{1}{2}\lambda_1(\Phi_1^\dagger\Phi_1)^2+\frac{1}{2}\lambda_2(\Phi_2^\dagger\Phi_2)^2+\lambda_3(\Phi_1^\dagger\Phi_1)(\Phi_2^\dagger\Phi_2)\\
&\qquad+\lambda_4(\Phi_1^\dagger\Phi_2)(\Phi_2^\dagger\Phi_1)+\left(\frac{1}{2}\lambda_5(\Phi_1^\dagger\Phi_2)^2+(\lambda_6(\Phi_1^\dagger\Phi_1)\right.\\
&\qquad\left.+\lambda_7(\Phi_2^\dagger\Phi_2))(\Phi_1^\dagger\Phi_2)+\text{H.c.}\right),
\end{aligned}
\tag{1}
$$

where all the parameters are assumed to be real,[3] including the vacuum expectation values (VEVs) of the scalar fields, hence there is no CP-violation. In general, by introducing some discrete symmetry $\Phi_1 \to \Phi_1$ and $\Phi_2 \to -\Phi_2$, the scalar potential does not have the contributions of λ_6 and λ_7.

It has long been proposed that there are four possibilities to satisfy the Paschos-Glashow-Weinberg theorem [68] in 2HDMs [11,12]. These are defined as follows: Type I (where one Higgs doublet couples to all fermions); Type-II (where one Higgs doublet couples to up-type quarks and the other to down-type ones); Type-X (also called "Lepton-specific," where the quark couplings are Type-I and the lepton ones Type-II); Type Y (also called "Flipped" model, where the quark couplings are Type II and the lepton ones Type-I). With these two scalar doublets, there are eight fields but only five of them are physical (pseudo)scalar ("Higgs") fields, which correspond to: two neutral CP-even bosons h(lighter)/H(heavier), one neutral CP-odd boson A and two charged bosons $H^\pm$. The mixing angle α of the two neutral CP -even bosons h and H is another parameter of the 2HDM model. In total, the 2HDM model can be described by the parameters α, β (where $\tan\beta$ is the ratio of the VEVs of the two Higgs doublet fields) and the masses of the five Higgs particles. With these inputs one can estimate all the parameters that are present in the scalar potential, to be specific, the λ's. These λ's (together with various scalar mass parameters) enter the expressions of the theoretical constraints like: vacuum stability, unitarity, perturbativity and also various EW precision observables (EWPOs), for example, the oblique parameters. All these 2HDM types are fully compatible with the SM-like Higgs boson discovery.

The flavor sector of 2HDMs is testable in low as well as in high energy collider experiments. The tests have been carried out in the most general version of a 2HDM with a Yukawa four-zero texture, wherein the Yukawa couplings are proportional to the geometric mean of two fermions masses, $g_{ij} \propto \sqrt{(m_i m_j)}\chi_{ij}$ [25,69,70]. As it was mentioned, a consequence of this is that the terms of the scalar potential including λ_6 and λ_7 should now be taken into account. This leads to tri-linear and quartic self-couplings of the scalar fields [18,22] affecting the model phenomenology in one loop processes via di-Higgs and tri-Higgs topologies, both in production and decay processes. It has been shown that the EWPO ρ can deviate from experimental bounds at one loop level, as long as the mass difference between charged Higgs bosons with CP-even/CP-odd masses is large, irrespective of the value of λ_6 and λ_7. Hence, some level of degeneracy between one neutral and the charged Higgs states is a precondition on the 2HDM spectra. In our construction, the Yukawa Lagrangian [20] is given by:

$$
\begin{aligned}
\mathcal{L}_Y=&-(Y_1^u\bar{Q}_L\tilde{\Phi}_1u_R+Y_2^u\bar{Q}_L\tilde{\Phi}_2u_R+Y_1^d\bar{Q}_L\Phi_1d_R\\
&+Y_2^d\bar{Q}_L\Phi_2d_R+Y_1^l\bar{L_L}\Phi_1l_R+Y_2^l\bar{L_L}\Phi_2l_R),
\end{aligned}
\tag{2}
$$

where $\Phi_{1,2}=(\phi_{1,2}^+,\phi_{1,2}^0)^T$ refer to the two Higgs doublets, $\tilde{\Phi}_{1,2}=i\sigma_2\Phi_{1,2}^*$. Besides, the fermion mass matrices after EW symmetry breaking are given, from Eq. (2), by: $M_f=\frac{1}{\sqrt{2}}(v_1Y_1^f+v_2Y_2^f)$, $f=u,\ d,\ l$, assuming that both Yukawa matrices Y_1^f and Y_2^f have the four-zero-texture form and are Hermitian [71]. After diagonalization, $\bar{M}_f=V_{fL}^\dagger M_f V_{fR}$, one has $\bar{M}_f=\frac{1}{\sqrt{2}}(v_1\tilde{Y}_1^f+v_2\tilde{Y}_2^f)$, where $\tilde{Y}_i^f=V_{fL}^\dagger Y_i^f V_{fR}$. One can obtain a compact and generic form for the rotated matrix $\tilde{Y}_n^f$[4]:

$$
[\tilde{Y}_n^f]_{ij}=\frac{\sqrt{m_i^f m_j^f}}{v}[\tilde{\chi}_n^f]_{ij}=\frac{\sqrt{m_i^f m_j^f}}{v}[\chi_n^f]_{ij}e^{i\vartheta_{ij}^f},
\tag{3}
$$

where the χ's are unknown dimensionless parameters of the model. Following [20], one has a generic expression for the couplings of the Higgs bosons to the fermions given as

$$
\begin{aligned}
\mathcal{L}^{\bar{f}_i f_j\phi}=&-\left\{\frac{\sqrt{2}}{v}\bar{u}_i(m_{d_j}X_{ij}P_R+m_{u_i}Y_{ij}P_L)d_jH^+\right.\\
&\left.+\frac{\sqrt{2}m_{l_j}}{v}Z_{ij}\overline{\nu_L}l_RH^++\text{H.c.}\right\}\\
&-\frac{1}{v}\{\bar{f}_im_{f_i}h_{ij}^ff_jh^0+\bar{f}_im_{f_i}H_{ij}^ff_jH^0\\
&-i\bar{f}_im_{f_i}A_{ij}^ff_j\gamma_5A^0\},
\end{aligned}
\tag{4}
$$

where ϕ_{ij}^f ($\phi=h,\ H,\ A$), X_{ij}, Y_{ij} and Z_{ij} are defined as follows:

[3]The μ_{12}^2, λ_5, λ_6 and λ_7 parameters could be complex in general, but for simplicity we assume these parameters to be real.

[4]We have shown in several parametrizations that this structure corresponds, as a particular case, to the Cheng and Sher ansatz [19,20,25,70].

TABLE I. Parameters for few optimistic benchmark points in the 2HDM-III as a 2HDM-I, -II and -Y configuration. Here bs stands for $\mathrm{BR}(\phi \to b\bar{s} + \bar{b}s)$, in units of 10^{-2}, where $\phi = h, H$, while $\sigma.bs$ stands for the cross section multiplied by the above BR as obtained at the LHeC in units of fb. We have analyzed only the benchmarks where the $\sigma.bs$ is greater than 0.15 fb, so that at least 15 events are produced for 100 fb^{-1}.

				$m_h = 125$ GeV		$m_H = 130$ GeV		$m_H = 150$ GeV		$m_H = 170$ GeV	
2HDM	X	Y	Z	bs	$\sigma.bs$	bs	$\sigma.bs$	bs	$\sigma.bs$	bs	$\sigma.bs$
Ib35	28	10	28	15.66	6.392	51.8	1.209	51.6	0.30	1.58	0.117
Ib47	30	5	30	16.14	3.086	48.2	10.983	48.0	0.127	1.80	0.839
Ib57	44	5	44	17.58	11.861	38.6	5.14	38.4	2.303	3.68	0.137
IIa11	20	2	20	1.42	1.055	25.2	0.097	25.0	0.091	24.8	0.085
IIa14	26	2	26	1.44	1.651	26.0	0.059	25.8	0.054	25.6	0.049
IIa26	36	1	36	1.46	1.621	26.4	0.045	26.2	0.042	26.0	0.038
Ya11	20	2	−2	1.42	1.084	25.2	0.062	25.0	0.059	24.8	0.054
Ya12	22	2	−2	1.44	1.078	25.6	0.057	25.4	0.053	25.2	0.048
Ya14	26	2	−2	1.46	1.441	26.0	0.057	25.8	0.053	25.6	0.049

$$h^d_{ij} = \xi^d_h \delta_{ij} + \frac{(\xi^d_H - X\xi^d_h)}{\sqrt{2} f(X)} \sqrt{\frac{m_{d_j}}{m_{d_i}}} \tilde{\chi}^d_{ij},$$
$$h^\ell_{ij} = h^d_{ij}(d \to \ell, X \to Z), \tag{5}$$

$$H^d_{ij} = \xi^d_H \delta_{ij} - \frac{(\xi^d_h + X\xi^d_H)}{\sqrt{2} f(X)} \sqrt{\frac{m_{d_j}}{m_{d_i}}} \tilde{\chi}^d_{ij},$$
$$H^\ell_{ij} = H^d_{ij}(d \to \ell, X \to Z), \tag{6}$$

$$A^d_{ij} = -X\delta_{ij} + \frac{f(X)}{\sqrt{2}} \sqrt{\frac{m_{d_j}}{m_{d_i}}} \tilde{\chi}^d_{ij},$$
$$A^\ell_{ij} = A^d_{ij}(d \to \ell, X \to Z),$$
$$A^u_{ij} = A^d_{ij}(d \to u, X \to Y), \tag{7}$$

$$h^u_{ij} = \xi^u_h \delta_{ij} - \frac{(\xi^u_H + Y\xi^u_h)}{\sqrt{2} f(Y)} \sqrt{\frac{m_{u_j}}{m_{u_i}}} \tilde{\chi}^u_{ij},$$
$$H^u_{ij} = \xi^u_H \delta_{ij} + \frac{(\xi^u_h - Y\xi^u_H)}{\sqrt{2} f(Y)} \sqrt{\frac{m_{u_j}}{m_{u_i}}} \tilde{\chi}^u_{ij}, \tag{8}$$

$$X_{ij} = \sum_{l=1}^{3} (V_{\mathrm{CKM}})_{il} \left[X \frac{m_{d_l}}{m_{d_j}} \delta_{lj} - \frac{f(X)}{\sqrt{2}} \sqrt{\frac{m_{d_l}}{m_{d_j}}} \tilde{\chi}^d_{lj} \right], \tag{9}$$

$$Y_{ij} = \sum_{l=1}^{3} \left[Y\delta_{il} - \frac{f(Y)}{\sqrt{2}} \sqrt{\frac{m_{u_l}}{m_{u_i}}} \tilde{\chi}^u_{il} \right] (V_{\mathrm{CKM}})_{lj}, \tag{10}$$

$$Z^l_{ij} = \left[Z \frac{m_{l_i}}{m_{l_j}} \delta_{ij} - \frac{f(Z)}{\sqrt{2}} \sqrt{\frac{m_{l_i}}{m_{l_j}}} \tilde{\chi}^l_{ij} \right], \tag{11}$$

where $f(x) = \sqrt{1 + x^2}$, ξ^f_ϕ are related to the trigonometric ratios (i.e., $\cos\alpha/\sin\beta$, $\sin\alpha/\sin\beta$, $\cos\alpha/\cos\beta$, $\sin\alpha/\cos\beta$) and the parameters X, Y, and Z can be related to $\tan\beta$ or $\cot\beta$, according to the various incarnations of 2HDMs [20]. Taking into account that the Higgs-fermion-fermion (ϕff) coupling in the 2HDM-III is written as $g^{\phi ff}_{\text{2HDM-III}} = g^{\phi ff}_{\text{2HDM-any}} + \Delta g$, where $g^{\phi ff}_{\text{2HDM-any}}$ is the coupling ϕff in some of the 2HDMs with discrete symmetry and Δg is the contribution of the four-zero texture,[5] it was pointed out in [20] that this Lagrangian could also represent a multi-Higgs doublet model (MHDM) [72] or an aligned 2HDM (A2HDM) [13] with additional flavor physics in the Yukawa matrices.

In the case of the decay of neutral Higgs bosons, the diagrams which contribute involve only vertices like $t\bar{t}$, $t\bar{c}$, $t\bar{u}$, $c\bar{u}$, $b\bar{b}$, $b\bar{s}$, $b\bar{d}$, $s\bar{d}$ in the quark sector. In almost all the different versions of the 2HDM, except the lepton specific, the most relevant Higgs boson decay diagrams are those in which one has the couplings $b\bar{b}$ and $b\bar{s}$. It is clear that those diagrams containing the top quark in the final state are kinematically not allowed. Further, the fermion flavor violating amplitudes in the 2HDMs are proportional to $(X\sqrt{m_q m_{q'}})$ for quarks and $(Z\sqrt{m_\ell m_{\ell'}})$ for leptons [see Eqs. (4)–(6) and Table I]. Therefore the only relevant diagram which violates fermion flavor is that containing the coupling $b\bar{s}$. In the case of the lepton specific model we should take care that the diagram for the subprocess $h^0 \to b\bar{s}$ is proportional to the parameter X and the subprocess $h^0 \to \tau\bar{\mu}$ is proportional to the parameter Z and this could make the contribution of the latter larger than the contribution of the former subprocess, because in this case it could happen that $Z \gg X$ when $\tan\beta$ is large.

Here, we consider three different incarnations of the 2HDM-III, which correspond to the four 2HDM types already described except the lepton specific one, as here leptonic branching ratios (BRs) are dominant, whereas we intend to look for an enhancement in the Higgs to $b\bar{s}$ decay because of flavor violation. We will finally show that, in

[5]For example, one can recovers the Yukawa interactions given in Refs. [72–74] with $\chi^f_{ij} = 0$.

different scenarios of the 2HDM-III, a substantial enhancement of the BR($\phi \to b\bar{s}$) (including charge conjugation) is possible. We do so first via a parameter scan of the 2HDM-III at the inclusive level, followed by the detailed event generation analysis of some benchmark scenarios amenable to phenomenological investigation.

III. THE 2HDM-III PARAMETERS AND BENCHMARKS

In this section, we will perform a parameter scan of the 2HDM-III of interest from which we will extract our benchmark scenarios, all of which will be studied in our final signal-to-background simulations, albeit we will show detailed results only for a subset of these for reasons of space.

First, we ought to explain the constraints we have enforced in our analysis. As for the experimental ones, we have taken into account recent experimental bounds from flavor physics [13,20]: i.e., from $B \to \tau\nu_\tau$, $D \to \mu\nu$, $D_s \to \ell\nu$, the semileptonic transition $B \to D\tau\nu_\tau$, the inclusive decay $B \to X_s\gamma$, $B_0 - B_0$ mixing, $B_s \to \mu^+\mu^-$ and the radiative decay $Z \to b\bar{b}$. (We have also imposed EWPO limits.) On the theoretical side, we have enforced perturbativity, triviality, vacuum stability and unitarity constraints [18,75]. In all the constraints mentioned above, the charged Higgs bosons masses are the crucial parameter, as diagrams with $H^\pm$ states coexist alongside those involving the SM $W^\pm$ exchange diagrams. In this connection, alongside flavor and EWPO constraints, we have also accounted for those stemming from Tevatron and LHC searches [20,76–78].[6]

A. Parameter scan

We scan the parameters space of the model and we only consider as viable the points that avoid the aforementioned theoretical and experimental bounds and that are fully consistent with the most recent results of Higgs physics from LHC. Taking into account that our model provides interesting new physics in the form of a substantial enhancement of the decay $\phi \to s\bar{b} + \text{H.c.}$ ($\phi = h, H$), as a direct consequence of the off-diagonal terms of the texture of the Yukawa matrices. In our scanning, we ask that BR($\phi \to s\bar{b} + \text{H.c.}$) ~ 0.01 to 0.1, keeping the decay $\phi \to b\bar{b}$ dominant. First, we scan the off-diagonal terms of the Yukawa matrices and after we chose some interesting sets of the χ's parameters, which are consistent with the flavor physics constraints and Higgs physics bounds used in the analysis of [19–21], where we have shown that several meson-physics processes are very sensitive to charged Higgs boson exchange, and the off-diagonal terms of Yukawa matrices given in the Eq. (3) are kept constrained in the following range:

$$-0.06 \le (\chi_n^d)_{23} \le 0.3, \qquad -0.3 \le (\chi_n^u)_{23} \le 0.5. \quad (12)$$

Second, we fix the χ's parameters and the masses of the following Higgs bosons, $m_h = 125$ GeV, $m_A = 100$ GeV and $m_{H^\pm} = 110$ GeV. We run the mass m_H of the Higgs boson H from 130 GeV up to 200 GeV. Therefore, we can reduce the study of the parameter space to that of the couplings X and Y only, which are constrained strongly by the inclusive radiative decay $B \to X_s\gamma$ through the following bound:

$$-1.7 \le \text{Re}\left(\frac{X_{33}Y_{32}}{V_{tb}V_{Vts}}\right) \le 0.3, \quad (13)$$

where X_{33}, Y_{32} are defined in Eqs. (9)–(10) and V_{tb} and V_{ts} are elements of the Cabibbo-Kobayashi-Maskawa (CKM) matrix. From the constraint in Eq. (13), we can define the allowed region for two general cases. (a) For the case I defined by: $X = -Y$ or $X = Y$, $0.1 \le \cos(\beta - \alpha) \le 0.5$, and fixing the parameters of Yukawa matrices, $\chi^u_{kk} = 1.5$ ($k = 2, 3$), $\chi^d_{22} = 1.8$, $\chi^d_{33} = 1.2$, $\chi^{u,d}_{23} = 0.2$, $\chi^\ell_{22} = 0.5$, $\chi^\ell_{33} = 1.2$, $\chi^\ell_{23} = 0.1$. One can see in Fig. 1 in the left panel the allowed region for $Y = -X \le 15$ and for the case $X = Y \le 20$. This region could represent the case of the 2HDM-I plus a deviation given for the flavor symmetry of the Yuwaka matrices. (b) For the case II given by: $X \gg Y$, with $\cos(\beta - \alpha) = 0.1$, $\chi^u_{22} = 0.5$, $\chi^u_{33} = 1.4$, $\chi^d_{22} = 2$, $\chi^d_{33} = 1.3$, $\chi^u_{23} = -0.53$, $\chi^d_{23} = 0.2$, $\chi^\ell_{22} = 0.4$, $\chi^\ell_{33} = 1.2$, we can see that the large values for parameter X are permitted. This case could be the incarnation of both the 2HDM-II and 2HDM-Y (or flipped model) plus a deviation given by the four-zero texture of the Yukawa matrices. Considering these criteria, we chose three interesting scenarios from the versions of 2HDM-III: *Scenario Ib* which is related to the 2HDM-I-Like, with $\cos(\beta) = 0.5$, *Scenario IIa* is the case 2HDM-II-like, with $\cos(\beta) = 0.1$, and *Scenario Ya* is the case 2HDM-Y-like, with $\cos(\beta) = 0.1$.

B. Benchmark scenarios

Taking in account the scan of the parameters space, we chose the benchmark scenarios, where their main features can be recapped as follows:

(i) *Scenario Ib*: 2HDM-III as 2HDM-I, with the couplings ϕff given by $g^{\phi ff}_{\text{2HDM-III}} = g^{\phi ff}_{\text{2HDM-I}} + \Delta g$ and $\cos(\beta - \alpha) = 0.5$, $\chi^u_{kk} = 1.5$ ($k = 2, 3$), $\chi^d_{22} = 1.8$, $\chi^d_{33} = 1.2$, $\chi^{u,d}_{23} = 0.2$, $\chi^\ell_{22} = 0.5$, $\chi^\ell_{33} = 1.2$, $\chi^\ell_{23} = 0.1$, $m_A = 100$ GeV and $m_{H^\pm} = 110$ GeV, taking X and Y located in the blue region of the left panel from Fig. 1.

(ii) *Scenario IIa*: 2HDM-III as 2HDM-II, namely, the couplings ϕff given by $g^{\phi ff}_{\text{2HDM-III}} = g^{\phi ff}_{\text{2HDM-II}} + \Delta g$ and $\cos(\beta - \alpha) = 0.1$, $\chi^u_{22} = 0.5$, $\chi^u_{33} = 1.4$, $\chi^d_{22} = 2$, $\chi^d_{33} = 1.3$, $\chi^u_{23} = -0.53$, $\chi^d_{23} = 0.2$, $\chi^\ell_{22} = 0.4$, $\chi^\ell_{33} = 1.2$, $\chi^\ell_{23} = 0.1$, $m_A = 100$ GeV and $m_{H^\pm} = 110$ GeV, taking X and Y allowed in the right panel of Fig. 1.

[6] Current low energy constraints on the Higgs boson masses have been studied very recently [79,80].

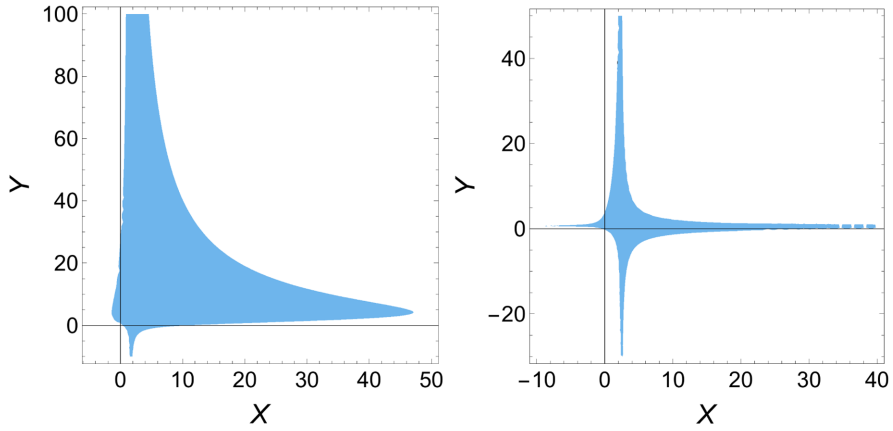

FIG. 1. The allowed region in the plane X vs Y, using the constraint Eq. (13), which is obtained from the radiative inclusive decay $B \to X_s\gamma$. We obtain the Scenario Ib, which is shown in the left panel, with $0.1 \leq \cos(\beta-\alpha) \leq 0.5$, $\chi^u_{kk} = 1.5$ $(k = 2, 3)$, $\chi^d_{22} = 1.8$, $\chi^d_{33} = 1.2$, $\chi^{u,d}_{23} = 0.2$, $\chi^\ell_{22} = 0.5$, $\chi^\ell_{33} = 1.2$, $\chi^\ell_{23} = 0.1$. For Scenario IIa and Y, the allowed region is given in the right panel with $\cos(\beta-\alpha) = 0.1$, $\chi^u_{22} = 0.5$, $\chi^u_{33} = 1.4$, $\chi^d_{22} = 2$, $\chi^d_{33} = 1.3$, $\chi^u_{23} = -0.53$, $\chi^d_{23} = 0.2$, $\chi^\ell_{22} = 0.4$, $\chi^\ell_{33} = 1.2$, $\chi^\ell_{23} = 0.1$. For both cases $m_h = 125$ GeV, 130 GeV $\leq m_H \leq 300$ GeV, 100 GeV $\leq m_A \leq 250$ GeV, 110 GeV $\leq m_{H^\pm} \leq 200$ GeV.

(iii) *Scenario Y*: 2HDM-III as 2HDM-Y, namely, the couplings ϕff given by $g^{\phi ff}_{\text{2HDM-III}} = g^{\phi ff}_{\text{2HDM-Y}} + \Delta g$ and $\cos(\beta-\alpha) = 0.1$, $\chi^u_{22} = 0.5$, $\chi^u_{33} = 1.4$, $\chi^d_{22} = 2$, $\chi^d_{33} = 1.3$, $\chi^u_{23} = -0.53$, $\chi^d_{23} = 0.2$, $\chi^\ell_{22} = 0.4$, $\chi^\ell_{33} = 1.1$, $\chi^\ell_{23} = 0.1$, $m_A = 100$ GeV and $m_{H^\pm} = 110$ GeV, taking the same X and Y for the Scenario IIa.

Hereinafter, we only simulated benchmarks where $\sigma.\text{BR}(\phi \to b\bar{s})$ [cross section of the charged current production $\nu_e \phi q$ multiplied by branching ratio of the channel decay $\phi \to b\bar{s} + \text{c.c.}$, with $(\phi = h,\ H)$], are more than 0.15 fb so that, for an integrated luminosity of 100 fb^{-1}, we can start with at least 15 events. Finally, when producing differential spectra of physical observables, we will concentrate on three 2HDM scenarios where the number of Higgs signal events in the $b\bar{s} + \text{c.c.}$ mode are large enough in order to be able to appreciate the underlying dynamics.

IV. NUMERICAL ANALYSIS

In this section, we describe first the production of Higgs signal. We then discuss the most important SM backgrounds and the different kinematics selections on the simulated events.

A. Higgs bosons signals

We consider the leading production processes[7] of Higgs boson: $\nu_e \phi q$, where $\phi = h$ and H while q is a light-flavor quark (i.e., u, d, s, c). We assume that ϕ is dominantly decaying into $b\bar{s}$ (plus charge conjugation). So both of our signals, the lighter Higgs as well as the heavier Higgs one, contain three jet (one is forward and two are central), missing (transverse) energy and no-lepton. Out of the two central jets, one is b-tagged and the other is a light-flavor jet. We estimated the parton level signal cross sections with flavor-violation within the 2HDM-III by using CalcHEP [81]. This implementation also calculates the BRs of the Higgs boson ϕ into $b\bar{s}$. For estimating the cross sections at the LHeC [63,82–86], we consider an electron beam, of energy $E_{e^-} = 60$ GeV and a proton beam of energy $E_p = 7000$ GeV, corresponding to a center-of-mass energy of approximately $\sqrt{s} = 1.296$ TeV. The integrated luminosity is 100 fb^{-1}. To estimate the event rates at parton level we applied the following basic preselections:

$$p_T^q > 15 \text{ GeV}, \qquad \Delta R(q,q) > 0.4 \tag{14}$$

with $\Delta R = \Delta\eta^2 + \Delta\phi^2$, where η and ϕ are the pseudorapidity and azimuthal angle, respectively. We take $m_t = 173.3$ GeV as the top-quark pole mass. We set the renormalization and factorization scale at the Z-boson mass (which is approximately the momentum transfer scale for the signal) and adopt CTEQ6L [87] as parton distribution functions (PDFs), with α_s (the strong coupling constant) evaluated consistently at all stages (PDFs, hard scattering and decays).

Considering the latter, we calculate in the allowed regions given above in the Fig. 1, the event rates $(\sigma.\text{BR}.L)$ at parton level for the neutral Higgs bosons h and H in the Scenarios Ib, IIa and Y, respectively, considering both luminosities of 100 fb^{-1}, which are shown in Figs. 2–3. One can see that the blue region contains the best benchmark points for all scenarios. We show that the most optimistic is in fact Scenario Ib for both

[7]The charged-current production is approximately 5 times larger than the neutral current production. Moreover, the neutral current production contains an electron and, since we are vetoing leptons in this particular analysis, we consider only the charged processes.

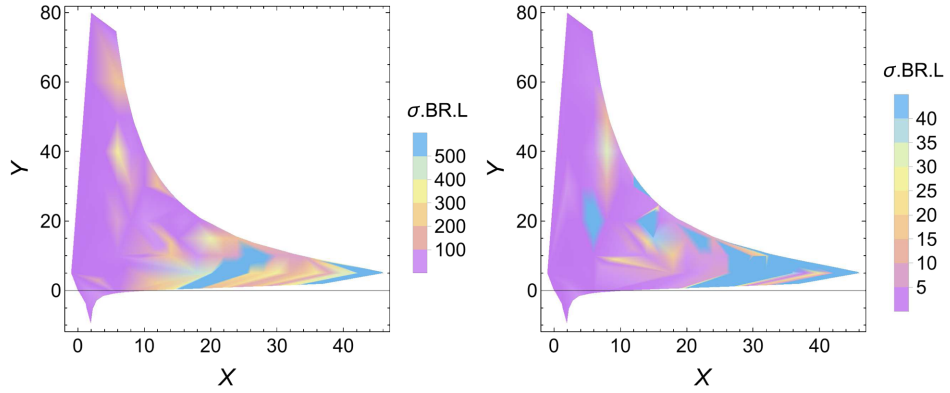

FIG. 2. Event rates (σ.BR.L) at parton level for the neutral Higgs boson h (left panel) and $m_H = 130$ GeV (right panel), where L is the integrated luminosity. We show Scenario Ib for 100 fb^{-1}. We consider $m_h = 125$ GeV.

Higgs bosons h and H, which reach events rates of order 500–1300 (5000–13000) with an integrated luminosity of 100 fb^{-1} (1000 fb^{-1}), although Scenarios IIa and Y also have some interesting benchmark points where one can obtain 17 events rates at the same luminosity. Table I shows the benchmark points that we select as interesting for studies at the LHeC. There are twenty-seven in total, obtained by taking the same three different values of the H mass ($m_H = 130$, 150, 170 GeV) in correspondence to nine different configurations of the other parameters. The products of cross sections times the relevant BRs ($\sigma.bs$) are shown in Table I.

Restricting ourselves to the points for which the inclusive event rates are most optimistic, all estimated by taking all the light-flavor quarks, the b-quark and the gluon as fluxes inside the proton and upon considering appropriate flavor-mixing where appropriate, we have then proceeded as follows. The top-quark and W-boson were allowed to decay freely as implemented in PYTHIA [88]. Following this, it was recognized that the signal processes have unique kinematic profiles. In particular, the final state quark transverse momentum is less than the mass of the vector bosons, its energy is very high with a small angle with respect to the beam directions (i.e., high forward rapidity). This will serve as guidance in our event selection. However, before proceeding further in this direction, we have to acknowledge at this point that these processes and their kinematic features to discover generic Higgs bosons have been studied for a long time [89–97]. Further parton level studies have been performed within the SM recently in [98]. In the context of BSM physics, cross section estimates while taking into account next-to-leading order (NLO) correction factors have been performed in [99] but no signal and background studies have been reported therein. In fact, dedicated simulations at the event generator level have not been done extensively and we focus here on these aspects, most importantly, with the intent of detecting two Higgs bosons simultaneously in novel flavor-violating modes.

B. Backgrounds

There are mainly two groups of SM noise to our Higgs signals. The charged-current backgrounds, $\nu t\bar{b}$, $\nu b\bar{b}j$, $\nu b2j$, $\nu 3j$, and the photo-production ones, $e^- b\bar{b}j$, $e^- t\bar{t}$. For estimating the cross sections of these SM backgrounds, we have used the same preselections like for the signal, Eq. (14), and identical conventions and parameter sets. The expected number of events for 100 fb^{-1} of integrated luminosity are given in the third column of Table II.

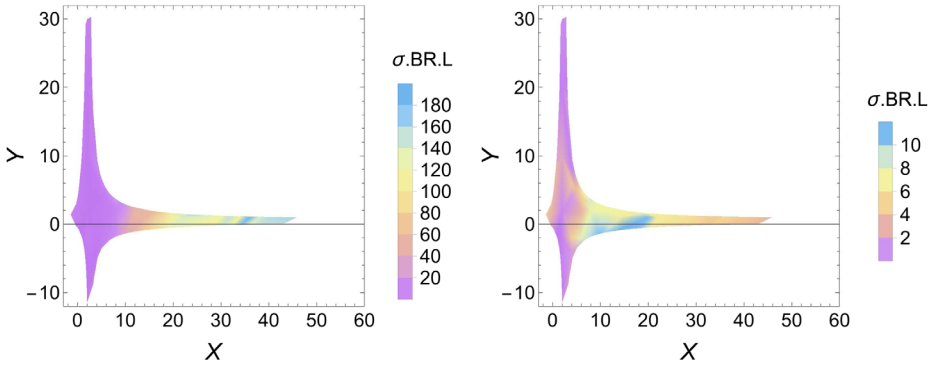

FIG. 3. The same as Fig. 2, but now for the Scenario IIa. Similar results for Scenario Y are obtained.

TABLE II. Expected number of events after different combinations of cuts for signal and backgrounds at the LHeC with an integrated luminosity of 100 fb^{-1} for $m_h = 125$ GeV. SimEvt stands for the actual number of events analyzed in the Monte Carlo simulations. RawEvt stands for the number of events with only the generator–level cuts (14) imposed; for the signal as well as for background, these are calculated from the total cross section times branching ratio. In the final column we mention the significances($\mathcal{S}$) defined as $\mathcal{S} = S/\sqrt{B}$, where S stands for signal events, background events B for 100 fb^{-1} of data after all cuts mentioned in the "i" column. The number in the parenthesis in the final column represent the significances for 1000 fb^{-1}.

Proc	SimEvt	RawEvt	a	b	c	d	e	f	g	h	i	$\mathcal{S}$
Ib35	100 K	639.2	447.6	177.3	117.1	97.4	93.8	37.8	31.7	25.4	15.8	1.2(3.8)
Ib47	100 K	308.6	216.8	85.1	56.2	47.1	45.5	18.4	15.6	13.0	8.1	0.62(2.0)
Ib57	100 K	1186.1	833.7	325.7	215.5	180.6	173.9	70.3	59.1	49.3	31.1	2.4(7.5)
IIa11	100 K	105.5	74.3	29.1	19.2	16.0	15.4	6.3	5.3	4.4	2.8	0.21(0.70)
IIa14	100 K	165.1	116.1	45.2	30.0	25.4	24.4	9.7	8.3	6.9	4.4	0.33(1.05)
IIa26	100 K	162.1	114.4	44.7	29.5	24.5	23.6	9.5	8.1	6.8	4.3	0.33(1.03)
Ya11	100 K	108.4	76.3	29.8	19.6	16.4	15.8	6.4	5.4	4.6	2.9	0.22(0.70)
Ya12	100 K	107.8	76.2	29.6	19.5	16.3	15.7	6.3	5.4	4.5	2.8	0.21(0.67)
Ya14	100 K	144.1	101.7	39.8	26.0	21.7	20.8	8.2	7.0	5.9	3.8	0.29(0.92)
$\nu t\bar{b}$	100 K	50712.1	28338.4	15293.7	9845.0	8144.2	7532.7	2982.1	2058.0	652.2	139.6	
$\nu b\bar{b}j$	560 K	14104.6	6122.8	3656.7	1858.5	1787.1	1650.1	257.5	152.5	85.2	15.1	
$\nu b2j$	90 K	18043.1	8389.2	3013.0	1691.5	1445.5	1373.7	389.5	206.1	77.2	11.3	$B = 170.8$
$\nu 3j$	300 K	948064.2	410393.4	15560.9	0.0	0.0	0.0	0.0	0.0	0.0	0.0	$\sqrt{B} = 13.1$
$eb\bar{b}j$	115 K	256730.1	55099.8	36353.6	12659.8	1432.0	200.7	54.1	24.8	18.0	4.5	
$et\bar{t}$	130 K	783.3	685.0	384.5	265.9	179.3	26.2	11.6	10.5	3.9	0.3	

C. Signal-to-background analysis

We passed the CalcHEP v3.4.7 [81] generated parton level event on to PYTHIA v.6.408 [88], which handles the parton shower (both initial and final), hadronization, heavy hadron decays, etc. The final state radiation smears the four-momentum of the jets, thus the invariant mass of the Higgs boson signal is less than the actual values considered in the event. We also took the experimental resolutions of the jet angles and energy using the toy calorimeter PYCELL, in accordance with the LHeC detector parameters, given in PYTHIA. This has some nontrivial effect since we used the invariant mass to isolate the Higgs signal. In our study we considered the LHC type calorimeter for the LHeC. Although in reality this is not the case, for example, unlike ATLAS and CMS, the electromagnetic and the hadronic calorimeter at the LHeC is not symmetric. However, since we are not doing detector simulation and also we are not considering cracks in the detectors, we applied symmetric large rapidity coverage for jets and leptons in our analysis. We expect that these assumptions hardly alter our findings. The detector parameters in the toy calorimeter module PYCELL are set according to the LHeC detector [84]. Specifically, we assume large calorimeter coverage $|\eta| < 5.5$, with segmentation (the number of division in η and ϕ are 320 and 200 respectively) $\Delta\eta \times \Delta\phi = 0.0359 \times 0.0314$. Further, we have used Gaussian energy resolution [82] for both leptons ($\ell = e, \mu$) and jets (labeled as j), with

$$\frac{\Delta E}{E} = \frac{a}{\sqrt{E}} \oplus b, \tag{15}$$

where $a = 0.32$, $b = 0.086$ for jets and $a = 0.085$, $b = 0.003$ for leptons and $\oplus$ means addition in quadrature. We have used a cone algorithm for the jet-finding algorithm, with jet radius $\Delta R(j) = \sqrt{\Delta\eta^2 + \Delta\phi^2} = 0.5$. Calorimeter cells with $E^{\rm cell}_{T,\rm min} \geq 5.0$ GeV are considered to be potential candidates for jet initiators. All cells with $E^{\rm cell}_{\rm T,min} \geq 1.0$ GeV were treated as part of the would-be jet. A jet is required to have minimum summed $E^{j}_{T,\rm min} \geq 15$ GeV and the jets are ordered in E_T. Leptons ($\ell = e, \mu$) are selected if they satisfy the requirements: $E^{\ell}_T \geq 15$ GeV and $|\eta^{\ell}| \leq 3.0$. In our jet finding algorithm we include leptons as parts of jets. Finally we separate them, putting some isolation criterion as follows: if we find a jet near a lepton, with $\Delta R(j - \ell) \leq 0.5$ and $0.8 \leq E^{j}_T/E^{\ell}_T \leq 1.2$, i.e. if the jet E_T is nearly identical to that of this lepton, the jet is removed from the list of jets and treated as a lepton. However, if we find a jet within $\Delta R(j - \ell) \leq 0.5$ of a lepton, whose E_T differs significantly from that of the lepton, the lepton is removed from the list of leptons. This isolation criterion mostly removes leptons from b or c decays. We reconstructed the missing (transverse) energy ($\not{E}_T$) from all observed particles and shown in left panel of Fig. 5. We have also calculated the same from the energy deposition in the calorimeter cells and found consistency between these two methods. Only jets with $|\eta^{j}| < 2.5$ and $E^{j}_T \geq 15$ GeV "matched" with a b-flavored hadron (B-hadron), i.e. with $\Delta R(j, B - \text{hadron}) < 0.2$ is considered to be "taggable." We assume that these jets are actually tagged with probability $\epsilon_b = 0.50$. We also adopted mistagging of non-b jets as b-jets and treated c-jets differently from the

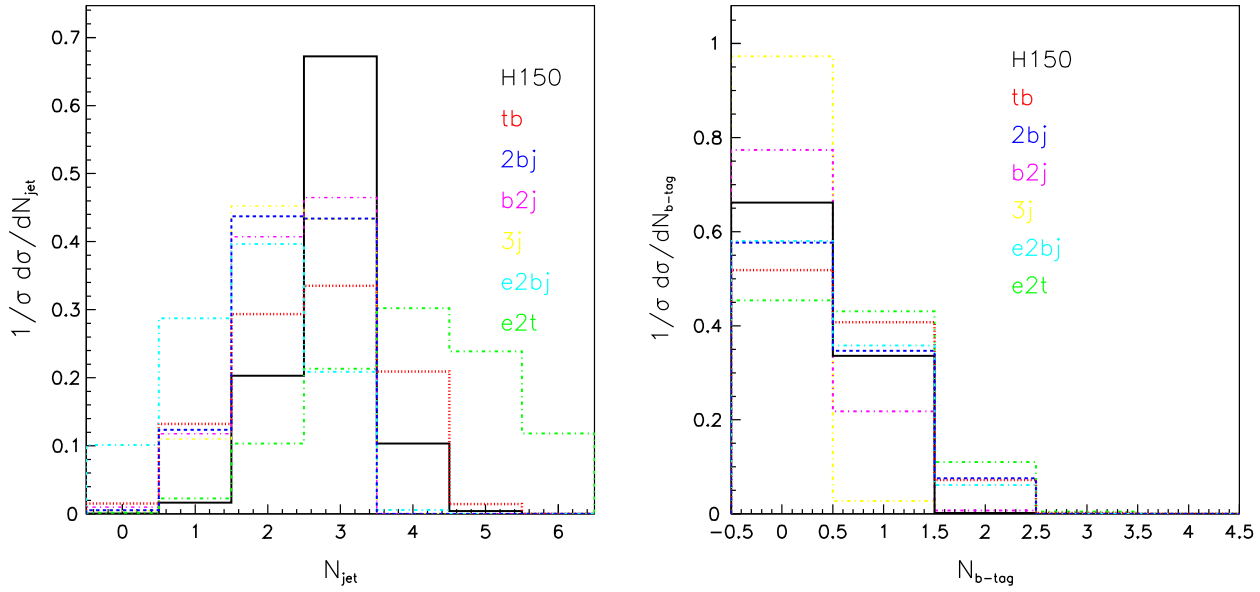

FIG. 4. Scenario Ib with the parameter $X = 28 = Z$ and $Y = 10$. The number of jets ($N_{\rm jet}$) in the left panel and the number of b-tagged jet with the inclusion of mis-tagging ($N_{b-\rm tag}$) in the right panel for signal ($m_H = 150$ GeV) and all the SM backgrounds. For other signal events, the distribution profiles are very similar, except the fact that the number of jets as well as b-tagged jets is slightly larger for heavy Higgs bosons. See the fourth(fifth) column for their actual efficiencies with selections applied in a(b) and A(B) for lighter(heavier) Higgs bosons, respectively.

gluon and light-flavor jets. A jet with $|\eta^j| \leq 2.5$ and $E_T^j \geq 15$ GeV matched with a c-flavored hadron (C-hadron, e.g., a D-meson or Λ_c-baryon), i.e., with $\Delta R(j, C - \text{hadron}) < 0.2$, is again considered to be taggable, with (mis-)tagging probability $\epsilon_c = 0.10$. Jets that are associated with a τ-lepton, with $\Delta R(j, \tau) \leq 0.2$, and all jets with $|\eta^j| > 2.5$, are taken to have vanishing tagging probability. All other jets with $E_T^j \geq 15$ GeV and $|\eta^j| \leq 2.5$ are assumed to be (mis-)tagged with probability $\epsilon_{u,d,s,g} = 0.01$. These efficiencies follow recent LHeC analyses [98].

The analysis strategy has been adopted from earlier work of some of us [100–102]. In particular, we have exploited a simple cut-based method for signal enhancement and background rejection. We have chosen the following selections and applied them cumulatively for the signal from h (H).

(i) *a(A):* We first selected events containing at least three jets (same). The distribution of the number of jet ($N_{\rm jet}$) is shown in the left panel of Fig. 4. For the lighter Higgs, h, in all the signal benchmarks the efficiencies[8] are approximately 70%(For heavier Higgs boson H, with mass of 130, 150 and 170 GeV the efficiencies are 71%, 76% 81% respectively, as two of the jets are directly coming from the corresponding heavier Higgs boson and hence the efficiencies are larger.). Further, $t\bar{b}$ has efficiency of approximately 56%, $2bj$ and $3j$ events display approximately 45% whereas the $b2j$ one has approximately 47%. Efficiencies are generally lower for the photo-production channels: $e2bj$ is approximately 20% (the sharp fall is due to the isolation criterion) whereas for $e2t$ the jet efficiencies are higher and due to the presence of two t-quarks leads to two b-quarks and the probability of having two jets from W-boson decay itself is approximately 91%, thus, out of 4-jets in 91% events, the probability of having at least three energetic jets is reduced by 4%, which leads to approximately 87% efficiency. However, as we will see, the presence of the electron in the photo-production modes leads to the corresponding backgrounds to be very low.

(ii) *b(B):* We demanded at least one b-tagged jet with the inclusion of proper mistagging (same). The distributions of the number of b-tagged jets ($N_{b-\rm tag}$) are shown in the right panel of Fig. 4. For the lighter Higgs, h, in all the signal benchmarks the b-tagging efficiencies are approximately 40%. In fact, all our signal benchmarks contain at least one b-quark and, since we adopted $\epsilon_b = 0.50$, the 10% lowering is quite realistic and due to the fact that not all b-quarks in the signal are eligible for the b-taggable criterion adopted in our analysis. For heavier Higgs signals, benchmarks show similar efficiencies and changes are less than 1% for three masses. In case of $t\bar{b}$, the events containing at least one b-tagged jet are approximately 54%, a rate greater than the signal

[8]Unless mentioned otherwise, all the efficiencies quoted hereafter are given with respect to the previous selection.

ones, as these background topologies contain at least two b-quarks at the parton level so that, due to combinatorics (other than mistagging a light-flavor quark-jet from W-boson decays), the probability of one b-tag is more. The probability of $2bj$ is approximately 60%, approximately 6% larger than $t\bar{b}$, due to, unlike $t\bar{b}$, the presence of one b-quark and one light-flavor jet in the hard processes. Further, $b2j$ efficiencies are similar to or little less than those of the signals due to the fact that the taggable rapidity is more central, where the jets are more likely to be forward in the basic hard processes. The efficiency of $e2t$ is approximately 2% larger than for $t\bar{b}$ mainly due to the contributions from mistagging one extra hadronic W, i.e, two extra jets. Finally, the efficiency of $3j$ is approximately 4%, which seems consistent with the expected mistagging rates (1.0% for light-flavor jets and 10% for c-jets) in presence of combinatorics.

(iii) *c(C):* We demanded at least two central jets, with $p_T > 30$ GeV ($p_T > 25$, 20 and 15 GeV for $m_H = 130$, 150 and 170 GeV, respectively[9]) in the pseudorapidity range $|\eta| < 2.5$. One of the central jet must be a b-tagged jet and we demanded only one b-tagged jet (same). For the lighter Higgs, h, all the signal benchmarks as well as the $t\bar{b}$ noise survive at the rate of approximately 65% since all these processes naturally have three jet in their events. Further, $e2bj$ and $2bj$ are reduced by approximately 35% and 50%, respectively, mainly due to demanding, with respect to the b(B) case above, of one b-tagged jet only. The diagrams of tb and $e2t$ reveal that these two backgrounds are more central, because of the presence of one t-quark in the central region. In fact, the efficiency is larger in $e2t$ and is mainly due to the contributions from the additional t-quark. Although in $2bj$ the probability in presence of one b-tagged in the central region is large the overall efficiency is reduced to 12% due to (partly) the possibility of more than one b-tagged jets whereas for Wb the value is mainly due to the hadronic branching fraction and also that the b-tagged jet is not necessary central. In case of $e2bj$ the efficiency is 35%: this noise suffers mainly due to the centrality criterion. For $3j$, none of the events survived this selection criterion. The efficiencies pattern discussed above are similar for the heavier Higgs boson, H, yet recall that here we have used slightly softer selections on the transverse momentum. Thus, the efficiencies are increasing with a softer p_T selection for both signals and backgrounds.

(iv) *d(D):* The missing transverse energy cut $\not{E}_T > 20$ GeV is first applied (same). The relevant distribution is shown in the left panel of Fig. 5. For all the signal benchmarks (lighter as well heavier Higgs bosons), $t\bar{b}$ and $b2j$ the efficiencies are approximately 83%. The sources of neutrinos and the event structures of these two processes are very similar, except for the fact that the top-quark decays produce either neutrinos (which are then pure sources of missing energy but in such a case, owing to the selection a(A), they are largely removed) or quarks (where the smearing of jets and track mismeasurements are the main sources of missing energy). For $2bj$ the efficiencies are approximately 96%. This selection is crucial to suppress the photoproduction processes: $e2bj$ and $e2t$. In case of $e2bj$ only 12% of the events survive in fact. For $e2t$ the presence of two W-bosons and their decays into leptonic modes would be the sources of missing energy, so that this noise is not affected very much by our constraints.

(v) *e(E):* A lepton (e or μ) veto for $p_T > 20$ GeV and $\eta < 3.0$ is applied here (same). For the lighter Higgs signal benchmarks, the efficiency for this selection is approximately 96%, as only 4% of the events contain at least one lepton which is coming from the semileptonic decays of B-hadrons and D-mesons and which passes the isolation criterion above. The efficiencies for $2bj$ and $b2j$ are rather close to the signal benchmarks, due to these processes also not having prompt leptons in their events. The $t\bar{b}$ channel has an efficiency of 93%, hence approximately 3% less than the signal, as here the top-quark decays can lead to one bottom-quark and, if the hard-processes bottom quarks are more central, the requirement in c(C) is satisfied and there is no problem in having a central and high-p_T lepton from a W-boson decay. In the photo-production processes, $e2bj$ and $e2t$ both contain hard leptons, so only 15% of the events survive our lepton veto. For heavier Higgs masses, the efficiencies are quite similar to the lighter Higgs boson mass case. The only difference is that, since the applied p_T threshold is lower for heavier Higgs masses, the probability of having a lepton in the event is higher, thus the veto efficiencies are somewhat smaller, except for the two photoproduction processes.

(vi) *f(F):* In the central region, defined above via c(C), we reconstruct the invariant mass of one b-tagged jet with any of the other jets, M_{bj}. Amongst these, we have chosen the best combination, i.e., where, the absolute difference $|M_{bj} - M_{h(H)}|$ is minimized. We call this dijet combination the candidate light (heavy) Higgs boson signal. In order to select the latter, we have kept events within a 15 GeV mass window centered around the corresponding Higgs boson masses. The distributions of M_{bj} are shown in the left panel of Fig. 6. It seems that the dijet

[9]Since the cross sections become smaller with increasing m_H, we lowered the central jet p_T cuts.

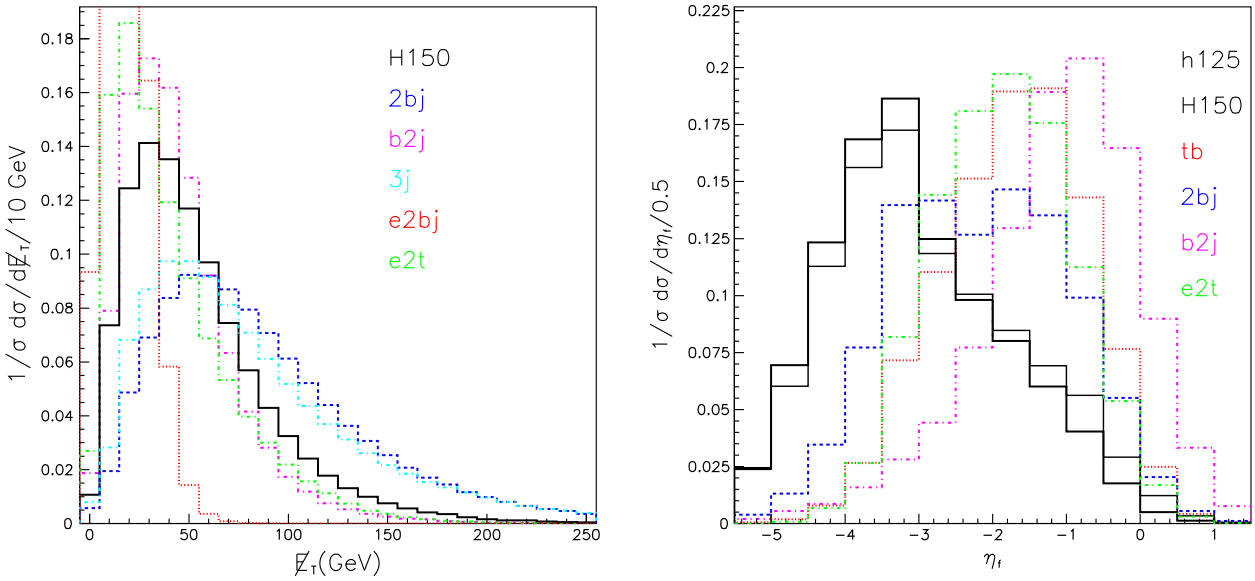

FIG. 5. The missing energy ($\not{E}_T$) (left panel) and rapidity (η_{j_f}) (right panel) profile of the forward jet for signals and SM backgrounds. The $\not{E}_T$ distributions for all other signal benchmarks as well as the $t\bar{b}$ noise are not shown as they are very similar to the signal distributions of $m_H = 150$ GeV for Scenario Ib with $X = Z = 28$ and $Y = 10$ (shown in thick solid), whereas the thin solid is for $m_h = 125$ GeV for Scenario Ia with $X = Z = 28$ with $Y = 10$. The rapidity distributions profile for $m_H = 130(170)$ GeV is very close to the $m_h = 125$ GeV($m_H = 130$ GeV) case shown in thin solid, except that for massive Higgs the peaks shift toward the left. Also the corresponding rapidity distribution profile for $e2bj$ is somewhat similar to the $m_h = 125$ GeV signal case.

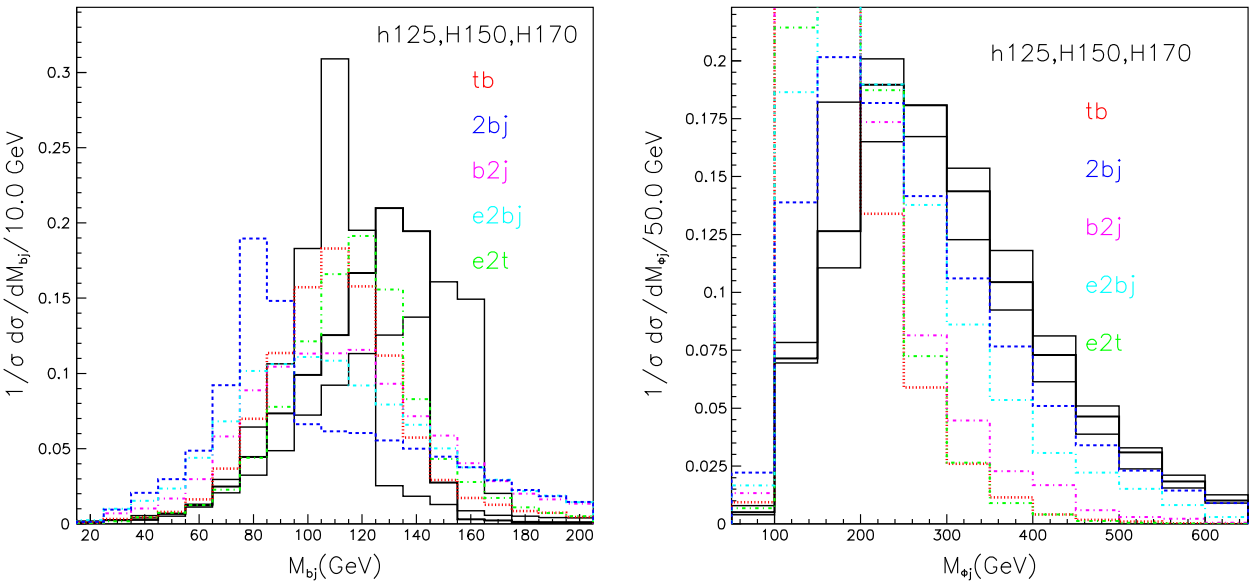

FIG. 6. The dijet invariant mass, made up by one b-tagged and one light-flavor jet, producing Higgs candidates, $M_\phi = M_{bj}$ (left panel) and the three-jet invariant mass, i.e., the previous two jets combined together with the forward jet, $M_{\phi j_f}$ (right panel). The mass peaks of the Higgs signals (M_ϕ) correspond to $m_h = 125$ (thin black) for Scenario Ia, $m_H = 150$ (thick black) and 170 (thin black) for Scenario Ib from left to right. All these are using the parameters $X = Z = 28$ and $Y = 10$. The distribution for $m_H = 130$ is not shown but it lies in between $m_h = 125$ and $m_H = 150$. Among all SM backgrounds, only $2bj$ shows a prominent peak from the Z-boson. Notice that $M_{\phi j_f}$ represents the overall energy scale of the hard-scattering.

invariant masses of the BP-Ia30 signal benchmark (with $m_h = 125$ GeV) has its peak around 115 GeV.[10] The distribution for $t\bar{b}$ also has a peak around that of the $m_h = 125$ GeV signal. However, the combinatorics is significant and this shows in their efficiencies, which are approximately 40% for both. The distribution of $b2j$ is flat as there is no correlations for the correct dijet candidates. Also note that $b2j$ has W-boson exchange resonant diagrams, so a probability in principle exists for a dijet invariant mass peak at M_W, however, this is very small, mainly due to low mistagging efficiencies and the centrality criterion. Further, also in case of $2bj$, where the Z-boson is present resonantly in the diagrams, the $Z \to b\bar{b}$ decay combined with high tagging efficiencies allows for the appearance of a dijet peak at 80 GeV (approximately 10 GeV less than M_Z due to jet energy smearing): see the left-panel of Fig. 6. In case of $e2t$, like $t\bar{b}$, one has also correlated dijet candidates, but the energy scale is higher, so the peak is shifted to higher masses. The efficiency is approximately 45%, a little larger than the signal and $t\bar{b}$ ones. The distributions of $b2j$ and $e2bj$ are flat and the efficiencies are the same, approximately 28%. This particular selection suppresses $2bj$ events more severely though, at a rate which is approximately 15%. For heavier Higgs bosons the distributions show rapid falls and so, by applying the mass window cuts, only the left part of the distributions contributes. This shows in their signal efficiencies, which are approximately 34%, 23% and 18% for $m_H = 130$, 150 and 170 GeV, respectively. The SM backgrounds do not show up in distributions at large invariant masses, thus for heavier Higgs mass combined with the same mass window selection suppresses more the backgrounds. As an example, in case of $e2t$, which produces somewhat higher invariant masses than all other SM backgrounds, the efficiencies drops to 40%, 12% and 4% for $m_H = 130$, 150 and 170 GeV, respectively. In case of $t\bar{b}$ the efficiencies (see Tables II–V) drop to from 30%, 8% and 2%, respectively. In case of $2bj$ the values are 14%, 10% and 5%. For $e2bj$, one has 20%, 10% and 7%, respectively. Finally, for $b2j$, these are 25%, 12% and 5%, respectively.

(vii) *g(G):* We demanded the remaining leading jet in the event to have $p_T > 25$ GeV, with $-5.5 < \eta < -0.5(-1.0)$ (these values are chosen by seeing the distribution, see the right panel of Fig. 5) and termed it as the forward jet (j_f). This forward jet lies very close to the direction of the incoming proton, like in vector boson fusion (VBF) processes for Higgs production. In contrast to VBF though, instead of a jet with large rapidity gap with respect the forward jet (a backward jet then), in our signal we have a neutrino. The more massive the Higgs is, the less energy remains for the forward jet so as to lay close to the proton direction, i.e., at larger rapidity. This reflects in the right panel of Fig. 5. The thick (thin) solid curve corresponds to $m_H = 150$ GeV ($m_h = 125$ GeV). For a lighter Higgs boson, $m_h = 125$ GeV, the efficiency is approximately 80%. For $e2t$ the efficiency is almost 90%, twice that of $e2bj$, as there is more than twice a probability to have a forward-jet from top-quark decays.

(viii) *h(H):* The dijet invariant mass of the Higgs boson candidates with the forward tagged jet, which is essentially the overall energy scale of the hard scattering, is asked to comply with the following requirements: m_{hj_f} (m_{Hj_f}) > 190 GeV (190, 210 and 230 GeV for $m_H = 130$, 150 and 170 GeV, respectively). The distributions are shown in the right panel of Fig. 6. For a lighter Higgs boson, $m_h = 125$ GeV, except a few cases,[11] the efficiency is approximately 82%. This forward jet should not be a b-jet though. So, in $t\bar{b}$ and $e2t$, where a forward b-tag jet is more probable, the efficiencies are lower, approximately 32% and 37%. It is clear from the right panel of Fig. 6 that the three-jet invariant mass distributions of $b2j$ peak around 140 GeV or so. The same for $t\bar{b}$, $e2t$, $2bj$, $e2bj$ and the Higgs signal with $m_h = 125$ GeV, which show somewhere around 180 GeV. So, for $m_h = 125$ GeV, the efficiency is around 82%. For the heavier Higgs boson, with $m_H = 150\,(170)$ GeV, the distributions are shown in the thick (thin) solid curve in the right panel of Fig. 6 and peak around 220 (260) GeV. The selection cuts for these two Higgs bosons are 210 and 230 GeV, respectively. With our selection, for these two heavy Higgs signals, one suppresses more SM backgrounds than in the case of the Higgs signal with $m_h = 125$ GeV and $m_H = 130$ GeV. For example, in the $t\bar{b}$ case, the most dominant background, for $m_h = 125$ GeV, and $m_H = 130$, 150 and 170 GeV, the events which survived are approximately 652, 618, 195 and 80, respectively. For other SM backgrounds a similar pattern follows, thus the overall SM backgrounds can be strongly reduced. However, this overall background rejection will not help alone to have larger significances as the signal rate itself is suppressed with heavier Higgs masses (at the production level).

[10]The peaks always show up to the left side of the actual masses due to jet energy smearing and the shift also depends on the jet-cone size.

[11]Recall that the efficiencies are relative to the previous selection, one can estimate the individual efficiencies from the respective distributions.

TABLE III. Same as Table II but for $m_H = 130$ GeV. The criterion for jets and b-tagging are the same, so that the number of events in column A and B are the same for all SM backgrounds.

Proc	SimEvt	RawEvt	A	B	C	D	E	F	G	H	I	$\mathcal{S}$
Ib35	100 K	120.9	87.1	34.1	26.9	22.5	21.6	7.5	6.1	5.3	3.4	0.28(0.88)
Ib47	100 K	1098.3	790.3	307.1	243.9	204.6	195.7	68.5	56.1	48.6	31.3	2.6(8.1)
Ib57	100 K	514.0	371.2	144.8	115.0	96.0	92.0	31.7	25.8	22.7	14.3	1.2(3.7)
IIa11	100 K	9.7	6.8	2.7	2.1	1.8	1.7	0.6	0.4	0.3	0.2	0.02(0.05)
IIa14	100 K	5.9	4.2	1.7	1.3	1.1	1.0	0.4	0.3	0.2	0.1	0.01(0.02)
IIa26	100 K	4.5	3.1	1.3	1.0	0.8	0.8	0.3	0.2	0.1	0.1	0.01(0.02)
Ya11	100 K	6.2	4.4	1.8	1.4	1.1	1.1	0.4	0.3	0.2	0.1	0.01(0.02)
Ya12	100 K	5.7	4.0	1.6	1.3	1.0	1.0	0.3	0.2	0.2	0.1	0.01(0.02)
Ya14	100 K	5.7	4.0	1.6	1.3	1.0	1.0	0.3	0.2	0.2	0.1	0.01(0.02)
$\nu t\bar{b}$	100 K	50712.1	28338.4	15293.7	10976.4	9092.4	8393.6	2550.9	1565.5	617.9	113.7	
$\nu b\bar{b}j$	560 K	14104.6	6122.8	3656.7	2145.5	2062.1	1902.9	266.6	141.0	87.5	14.4	
$\nu b2j$	90 K	18043.1	8389.2	3013.0	2053.6	1734.0	1650.1	402.8	143.7	64.5	8.1	$B = 147.8$
$\nu 3j$	300 K	948064.2	410393.4	15560.9	0.0	0.0	0.0	0.0	0.0	0.0	0.0	$\sqrt{B} = 12.2$
$eb\bar{b}j$	115 K	256730.1	55099.8	36353.6	16838.4	1826.6	284.1	56.4	31.6	22.6	11.3	
$et\bar{t}$	130 K	783.3	685.0	384.5	280.8	190.8	27.8	10.9	9.3	3.9	0.3	

(ix) *i(I):* Finally, we required only one light-flavor jet in the central region (same). This selection is called "central jet veto" and has severe impact on all processes having more jets in the central rapidity region, other than the Higgs candidate jets. Recall that our Higgs signal candidate jets, selected in f(F) above, are central: this is true for not only the signal, but also the dominant SM background, $t\bar{b}$. For a lighter SM Higgs, see Table II, approximately 35–40% of the events have a central jet other than Higgs candidate jets, thus only 60–65% of the events survive. For $t\bar{b}$, $\nu b2j$ and $\nu 2bj$ the efficiencies are 22%, 18% and 14%, respectively. Among all the SM backgrounds, $e2t$ has a larger number of jets (see the distributions in the left panel of Fig. 4), thus the probability of having a central jet is more, so that this selection suppresses this background severely, approximately by 93% (for all the Higgs cases, see Tabs. II–V).

After the cumulative selections from a–i, discussed above, we find that, for the SM Higgs boson with $m_h = 125$, the final number of events is around 15–30 only for Scenario Ib and for large values of the parameters $X = Z = 28(44)$ and $Y = 10(5)$ respectively. The total SM background rate is approximately 170. The charged-current backgrounds, $\nu t\bar{b}$, $\nu b\bar{b}j$ and $\nu b2j$, are the dominant ones and only 3% of the total background comes from $et\bar{t}$ photo-production. These rates lead to a maximum significance of approximately $2.4\,(7.5)\sigma$ with $100\,(1000)$ fb^{-1} integrated luminosity for Scenario Ib with $X = Z = 44$ and $Y = 5$. For Scenario Ib

TABLE IV. Same as Table III but for $m_H = 150$ GeV.

Proc	SimEvt	RawEvt	A	B	C	D	E	F	G	H	I	$\mathcal{S}$
Ib35	100 K	30.0	23.3	9.1	8.2	6.9	6.5	1.5	1.3	1.2	0.8	0.10(0.33)
Ib47	100 K	12.7	9.9	3.8	3.4	2.9	2.7	0.6	0.5	0.5	0.3	0.04(0.12)
Ib57	100 K	230.3	179.6	69.3	62.6	52.6	49.9	11.7	10.1	9.1	6.4	0.83(2.62)
IIa11	100 K	9.1	6.9	2.7	2.4	2.0	1.9	0.4	0.4	0.3	0.2	0.026(0.08)
IIa14	100 K	5.4	4.1	1.6	1.4	1.2	1.1	0.3	0.2	0.2	0.1	0.013(0.04)
IIa26	100 K	4.2	3.2	1.3	1.1	0.9	0.9	0.2	0.1	0.1	0.1	0.013(0.04)
Ya11	100 K	5.9	4.5	1.8	1.6	1.3	1.2	0.3	0.2	0.2	0.1	0.013(0.04)
Ya12	100 K	5.3	4.0	1.6	1.4	1.2	1.1	0.3	0.2	0.2	0.1	0.013(0.04)
Ya14	100 K	5.3	4.0	1.6	1.4	1.2	1.1	0.3	0.2	0.2	0.1	0.013(0.04)
$\nu t\bar{b}$	100 K	50712.1	28338.4	15293.7	11810.9	9808.7	9039.0	751.7	476.8	194.5	32.3	
$\nu b\bar{b}j$	560 K	14104.6	6122.8	3656.7	2395.6	2300.1	2120.8	199.3	112.4	70.8	12.4	
$\nu b2j$	90 K	18043.1	8389.2	3013.0	2427.2	2030.3	1933.1	234.2	83.7	41.0	6.3	$B = 60.1$
$\nu 3j$	300 K	948064.2	410393.4	15560.9	0.0	0.0	0.0	0.0	0.0	0.0	0.0	$\sqrt{B} = 7.7$
$eb\bar{b}j$	115 K	256730.1	55099.8	36353.6	21280.9	2270.8	385.6	36.1	24.8	20.3	9.0	
$et\bar{t}$	130 K	783.3	685.0	384.5	291.5	199.0	29.1	3.5	3.0	1.2	0.1	

TABLE V. Same as Table III but for $m_H = 170$ GeV.

Proc	SimEvt	RawEvt	A	B	C	D	E	F	G	H	I	$\mathcal{S}$
Ib35	100 K	11.7	9.6	3.7	3.5	3.0	2.8	0.5	0.4	0.4	0.3	0.053(0.17)
Ib47	100 K	83.9	69.2	26.7	25.5	21.5	20.2	3.6	3.1	3.0	2.2	0.39(1.23)
Ib57	100 K	13.7	11.2	4.3	4.1	3.4	3.2	0.6	0.5	0.5	0.4	0.07(0.22)
IIa11	100 K	8.5	7.0	2.7	2.5	2.1	2.0	0.3	0.3	0.3	0.2	0.035(0.11)
IIa14	100 K	4.9	4.1	1.6	1.5	1.3	1.2	0.3	0.17	0.16	0.12	0.021(0.07)
IIa26	100 K	3.8	3.1	1.2	1.1	0.9	0.9	0.1	0.1	0.1	0.1	0.02(0.06)
Ya11	100 K	5.4	4.4	1.7	1.6	1.4	1.3	0.2	0.2	0.2	0.1	0.02(0.06)
Ya12	100 K	4.8	4.0	1.5	1.4	1.2	1.1	0.2	0.2	0.2	0.1	0.02(0.06)
Ya14	100 K	4.9	4.0	1.6	1.5	1.2	1.1	0.2	0.2	0.1	0.1	0.02(0.06)
$\nu t\bar{b}$	100 K	50712.1	28338.4	15293.7	12381.7	10299.7	9465.2	209.7	144.5	75.9	13.2	
$\nu b\bar{b}j$	560 K	14104.6	6122.8	3656.7	2568.2	2465.8	2272.4	103.7	60.8	37.4	8.7	
$\nu b2j$	90 K	18043.1	8389.2	3013.0	2744.8	2278.1	2171.4	99.5	40.0	25.2	5.3	$B = 31.7$
$\nu 3j$	300 K	948064.2	410393.4	15560.9	0.0	0.0	0.0	0.0	0.0	0.0	0.0	$\sqrt{B} = 5.6$
$eb\bar{b}j$	115 K	256730.1	55099.8	36353.6	25010.7	2638.4	453.3	29.3	18.0	11.3	4.5	
$et\bar{t}$	130 K	783.3	685.0	384.5	298.8	204.5	29.9	1.0	0.8	0.5	0.0	

with $X = Z = 28$ and $Y = 10$, the significance is approximately $1.2\,(3.8)\sigma$ for $100\,(1000)$ fb^{-1} integrated luminosity. The significances for Scenario Y and Scenario IIa are less than 1. Thus, one can expect that Scenario Ib with large value of $X = 44 = Z$ and $Y = 5$ may be accessible through the SM-like Higgs boson signal already detected at the LHC.

We also searched for the second CP-even neutral Higgs boson of our 2HDM-III, with masses $m_H = 130$, 150 and 170 GeV. After the cumulative selections from A–I, the maximum number of signal events for $m_H = 130$ GeV is approximately 15 (30) and only for Scenario Ib with $X = Z = 44$ (30) with $Y = 5$. The total SM background is approximately 150. So the maximum significance is approximately $2.6\,(8.1)\sigma$ for $100\,(1000)$ fb^{-1} integrated luminosity. For the case $m_H = 150$ GeV, the number of signal events is approximately 7 and the SM background reduces to approximately 60: this leads to a significance of approximately $1.0(2.6)\sigma$ with $100\,(1000)$ fb^{-1} integrated luminosity. For $m_H = 170$ GeV, the raw event rate is approximately 80 to start with and, at the end, the count is only 2.[12] The total SM backgrounds is approximately 30, which leads to a significance approximately $0.4\,(1.23)\sigma$.

The LHeC will be operational for about ten years and expected to accumulate a total integrated luminosity of 1000 fb^{-1} of data. So, at the end of the run, we expect the SM Higgs boson will have 7.5σ (3.8σ) significance for Scenario Ib with $X = Z = 44$ (28) with $Y = 5(10)$. For Scenario IIa and Scenario Y, with $X = 26$ and $Y = 2$, the final significances are approximately 1σ. It seems that in all scenarios of the model, large X are favorable. For heavy Higgs masses with $m_H = 130$ GeV, for Scenario Ib with $X = 44$ and 30 with $Y = 5$, the maximal significances are approximately 8.1 and 3.7σ respectively. For $m_H = 150$ GeV, Scenario Ib with $X = 44$ and $Y = 5$, the final significance is 2.62σ. For $m_H = 170$ GeV, in the Scenario Ib with $X = 30$ and $Y = 5$, the final number of signal events is approximately 2. The estimated significances is 1.23σ. Thus, for high enough Higgs masses, one might invoke the aforementioned multivariate analyses to have larger significances.

[12]Note that our selection cuts applied above are not optimized. An increase of the luminosity is an easy solution from a phenomenological perspective. However, adopting multivariate analysis techniques must also be a better discriminator of signal from backgrounds.

V. CONCLUSIONS

After the discovery of a SM-like Higgs boson at LHC, one is well motivated to look for more of such states, which necessarily appear in BSM scenarios. Among the experimental facilities where more Higgs bosons can be searched for, one should list an ep collider which may be built at CERN, known as the LHeC. In our analysis we have considered a 2HDM-III with a four-zero Yukawa texture in three configurations, wherein both the SM-like Higgs boson and the heavier version of it can be accessible at the foreseen LHeC energy. We assumed that both of these states are decaying via a flavor-violating mode ($\phi \to b\bar{s}$). After a parameter scan, we have selected a few model benchmarks where the products of cross sections and flavor-violating BRs are large enough to produce sufficient events in which to look for both signatures. We studied the three-jet and missing energy channel, $3j + \not{E}_T$, from the charged-current production of $\nu_e \phi q_f$, where q_f is a forward jet with large rapidity and the other two jets come from the flavor-violating decay $\phi \to b\bar{s}$. We demanded one central jet to be b-tagged with the inclusion of the proper mistagging from light-flavor and gluon jets. We considered the most dominant SM backgrounds: charged-currents, $\nu t\bar{b}$, $\nu b\bar{b}j$, $\nu b2j$ and $\nu 3j$, and photo-production, $e^- b\bar{b}j$ and $e^- t\bar{t}$. We performed a full hadron–level Monte Carlo simulation

using CalcHEP as matrix element calculator, PYTHIA as parton shower/hadronization event generator and its PYCELL toy calorimeter in accordance with the LHeC detector parameters. We carefully implemented b-tagging, including mistagging of c-jets or light-flavor or gluon jets.

The signals under consideration do not have leptons, so we applied lepton vetos. The charged-current production has naturally missing energy due to the presence of neutrinos but no charged lepton. However, the photo-production processes have leptons in them but no direct missing energy (except the mis-measurements from jets and smearing), thus the missing energy selection together with the lepton veto suppressed the photo-production backgrounds to a very large extent.

The kinematics of the particular signals here considered is very interesting from the fact that the Higgs boson is produced in the central rapidity region and its decay daughters, one b-jet and one light-flavor jet, are also central. We reconstructed the invariant mass of this two jets and selected events only for masses within a 15 GeV window around the respective Higgs masses of the signal benchmarks. This selection reduces the SM backgrounds to a large extent and the invariant mass ensures the selection of flavor-violating decays. For massive Higgs bosons, although the signal event becomes low with the mass window selection, background suppression is more efficient.

As a next step of our selection, we identified the most energetic light-flavor forward jet (by seeing the rapidity profiles) and calculated the invariant mass with that jet together with the flavor-violating Higgs candidates jets. These three-jet invariant masses essentially give the overall energy scale of the hard scattering. Again, the more massive Higgs boson helps to suppress more SM backgrounds, in particular $\nu t\bar{b}$ and $et\bar{t}$, but the signal becomes smaller too.

At the end, the most important cut, we applied a central jet veto, i.e., we required one light-flavor central jet only. This suppresses SM backgrounds with large multiplicity, for example, $\nu t\bar{b}$ and $et\bar{t}$.

After all the selections, with 100 fb^{-1} of data, we found that the SM Higgs boson, h, would be detectable within the 2HDM-III in the scenario called in this work Ib with $X = Z = 44$ or 30 with $Y = 5$, with approximately 1-2σ. The heavier neutral Higgs boson, H, with masses 130 GeV (150 GeV), would have 2 (1)σ significances for large X and only for Scenario Ib.

The LHeC will be operational for around ten years and so it is expected to accumulate a total integrated luminosity of 1000 fb^{-1} of data. So, in all the cases mentioned above, the final significances will be enhanced. At the end of the run, the 2HDM-III Like-IIa (Like-Y) the SM Higgs will have 1σ. For $m_H = 130$ GeV, in the Scenario Ib with $X = 44$ (30) and $Y = 5$, the maximal significances are approximately 3.7 (8.1)σ. The maximal significances for $m_H = 150$ GeV is 2.6σ for Ib with $X = 44$ and $Y = 5$. For $m_H = 170$ GeV the final number of signal events is approximately 2, probably too little to be detected. However, it should be noted that we have adopted a simple cut-based method in this analysis. One would instead invoke more complex discriminators to enhance the significances within the designed luminosity, for example, multivariate analyses.

To conclude, after the first few years of the LHeC running, by adopting more complex discriminator and/or multivariate analyses, we expect that both h and H signals will appear at the LHeC.

ACKNOWLEDGMENTS

This work has been supported by SNI-CONACYT (México), VIEP-BUAP and by PRODEP-SEP (México) under the grant: "Red Temática: Física del Higgs y del Sabor". R. X. acknowledges the scholarship from CONACYT (México). S. M. is supported in part through the NExT Institute. S. P. D. is grateful to the post-doctoral fellowship and academic leave from Institute of Physics, Bhubaneswar, Odisha, India, while the project started.

[1] G. Aad *et al.* (ATLAS Collaboration), Observation of a new particle in the search for the Standard Model Higgs boson with the ATLAS detector at the LHC, Phys. Lett. B **716**, 1 (2012).

[2] S. Chatrchyan *et al.* (CMS Collaboration), Observation of a new boson at a mass of 125 GeV with the CMS experiment at the LHC, Phys. Lett. B **716**, 30 (2012).

[3] J. Adam *et al.* (MEG Collaboration), New constraint on the existence of the $\mu^+ \to e^+\gamma$ decay, Phys. Rev. Lett. **110**, 201801 (2013).

[4] B. Aubert *et al.* (*BABAR* Collaboration), Measurement of the semileptonic decays $B \to D\tau^-\bar{\nu}_\tau$ and $B \to D^{(*)}\tau^-\bar{\nu}_\tau$, Phys. Rev. D **79**, 092002 (2009).

[5] J. P. Lees *et al.* (*BABAR* Collaboration), Evidence for an Excess of $\bar{B} \to D^{(*)}\tau^-\bar{\nu}_\tau$ Decays, Phys. Rev. Lett. **109**, 101802 (2012).

[6] J. P. Lees *et al.* (*BABAR* Collaboration), Precision Measurement of the $B \to X_s\gamma$ Photon Energy Spectrum, Branching Fraction, and Direct CP Asymmetry $A_{CP}(B \to X_{s+d}\gamma)$, Phys. Rev. Lett. **109**, 191801 (2012).

[7] J. P. Lees *et al.* (*BABAR* Collaboration), Exclusive measurements of $b \to s\gamma$ transition rate and photon energy spectrum, Phys. Rev. D **86**, 052012 (2012).

[8] A. Matyja *et al.* (Belle Collaboration), Observation of $B \to D^{*-}\tau^+\bar{\nu}_\tau$ Decay at Belle, Phys. Rev. Lett. **99**, 191807 (2007).

[9] K. Abe *et al.* (Belle Collaboration), A measurement of the branching fraction for the inclusive $B \to X_s\gamma$ decays with BELLE, Phys. Lett. B **511**, 151 (2001).

[10] A. Limosani *et al.* (Belle Collaboration), Measurement of Inclusive Radiative B-meson Decays with a Photon Energy Threshold of 1.7-GeV, Phys. Rev. Lett. **103**, 241801 (2009).

[11] G. C. Branco, P. M. Ferreira, L. Lavoura, M. N. Rebelo, M. Sher, and J. P. Silva, Theory and phenomenology of two-Higgs-doublet models, Phys. Rep. **516**, 1 (2012).

[12] J. F. Gunion and H. E. Haber, The *CP* conserving two Higgs doublet model: The approach to the decoupling limit, Phys. Rev. D **67**, 075019 (2003).

[13] A. Pich and P. Tuzon, Yukawa alignment in the two-Higgs-doublet model, Phys. Rev. D **80**, 091702 (2009).

[14] Y. F. Zhou, Texture of Yukawa coupling matrices in general two Higgs doublet model, J. Phys. G **30**, 783 (2004).

[15] S. Kanemura, T. Ota, and K. Tsumura, Lepton flavor violation in Higgs boson decays under the rare tau decay results, Phys. Rev. D **73**, 016006 (2006).

[16] S. Kanemura, K. Matsuda, T. Ota, T. Shindou, E. Takasugi, and K. Tsumura, Search for lepton flavor violation in the Higgs boson decay at a linear collider, Phys. Lett. B **599**, 83 (2004).

[17] J. L. Diaz-Cruz, J. Hernandez–Sanchez, S. Moretti, R. Noriega-Papaqui, and A. Rosado, Yukawa textures and charged Higgs boson phenomenology in the 2HDM-III, Phys. Rev. D **79**, 095025 (2009).

[18] A. Cordero-Cid, J. Hernandez-Sanchez, C. G. Honorato, S. Moretti, M. A. Perez, and A. Rosado, Impact of a four-zero Yukawa texture on $h \to \gamma\gamma$ and γZ in the framework of the two Higgs doublet model type III, J. High Energy Phys. 07 (2014) 057.

[19] O. Felix-Beltran, F. Gonzalez-Canales, J. Hernandez-Sanchez, S. Moretti, R. Noriega-Papaqui, and A. Rosado, Analysis of the quark sector in the 2HDM with a four-zero Yukawa texture using the most recent data on the CKM matrix, Phys. Lett. B **742**, 347 (2015).

[20] J. Hernandez-Sanchez, S. Moretti, R. Noriega-Papaqui, and A. Rosado, Off-diagonal terms in Yukawa textures of the Type-III 2-Higgs doublet model and light charged Higgs boson phenomenology, J. High Energy Phys. 07 (2013) 044.

[21] J. Hernandez-Sanchez, S. Moretti, R. Noriega-Papaqui, and A. Rosado, Update of the 2HDM-III with a four-zero texture in the Yukawa matrices and phenomenology of the charged Higgs boson, *Proc. Sci.*, CHARGED 2012 (2012) 029 [arXiv:1302.0083].

[22] J. Hernandez-Sanchez, C. G. Honorato, M. A. Perez, and J. J. Toscano, The $\gamma\gamma \to \phi_i\phi_j$ processes in the Type-III two-Higgs-doublet model, Phys. Rev. D **85**, 015020 (2012).

[23] S. Moretti, A. Akeroyd, and J. Hernandez-Sanchez, $H^\pm \to cb$ in models with two or more Higgs doublets, *Proc. Sci.*, Charged 2014 (2014) 025 [arXiv:1409.7596].

[24] J. L. Diaz-Cruz, R. Noriega-Papaqui, and A. Rosado, Measuring the fermionic couplings of the Higgs boson at future colliders as a probe of a non-minimal flavor structure, Phys. Rev. D **71**, 015014 (2005).

[25] J. L. Diaz-Cruz, R. Noriega-Papaqui, and A. Rosado, Mass matrix ansatz and lepton flavor violation in the THDM-III, Phys. Rev. D **69**, 095002 (2004).

[26] J. L. Diaz-Cruz and J. J. Toscano, Lepton flavor violating decays of Higgs bosons beyond the standard model, Phys. Rev. D **62**, 116005 (2000).

[27] E. Arganda, A. M. Curiel, M. J. Herrero, and D. Temes, Lepton flavor violating Higgs boson decays from massive seesaw neutrinos, Phys. Rev. D **71**, 035011 (2005).

[28] G. Blankenburg, J. Ellis, and G. Isidori, Flavour-changing decays of a 125 GeV Higgs-like particle, Phys. Lett. B **712**, 386 (2012).

[29] R. Harnik, J. Kopp, and J. Zupan, Flavor violating Higgs decays, J. High Energy Phys. 03 (2013) 026.

[30] M. Arana-Catania, E. Arganda, and M. J. Herrero, Non-decoupling SUSY in LFV Higgs decays: a window to new physics at the LHC, J. High Energy Phys. 09 (2013) 160.

[31] E. Arganda, M. J. Herrero, X. Marcano, and C. Weiland, Imprints of massive inverse seesaw model neutrinos in lepton flavor violating Higgs boson decays, Phys. Rev. D **91**, 015001 (2015).

[32] S. Bressler, A. Dery, and A. Efrati, Asymmetric lepton-flavor violating Higgs boson decays, Phys. Rev. D **90**, 015025 (2014).

[33] E. Arganda, M. J. Herrero, X. Marcano, and C. Weiland, Radiatively-induced LFV Higgs Decays from Massive ISS Neutrinos, arXiv:1410.5779.

[34] J. Heeck, M. Holthausen, W. Rodejohann, and Y. Shimizu, Higgs $\to \mu\tau$ in Abelian and non-Abelian flavor symmetry models, Nucl. Phys. **B896**, 281 (2015).

[35] A. Crivellin, G. D'Ambrosio, and J. Heeck, Explaining $h \to \mu^\pm\tau^\mp$, $B \to K^*\mu^+\mu^-$ and $B \to K\mu^+\mu^-/B \to Ke^+e^-$ in a Two-Higgs-Doublet Model with Gauged $L_\mu - L_\tau$, Phys. Rev. Lett. **114**, 151801 (2015).

[36] D. Aristizabal Sierra and A. Vicente, Explaining the CMS Higgs flavor violating decay excess, Phys. Rev. D **90**, 115004 (2014).

[37] J. Kopp and M. Nardecchia, Flavor and *CP* violation in Higgs decays, J. High Energy Phys. 10 (2014) 156.

[38] A. Greljo, J. F. Kamenik, and J. Kopp, Disentangling flavor violation in the top-Higgs sector at the LHC, J. High Energy Phys. 07 (2014) 046.

[39] A. Dery, A. Efrati, Y. Nir, Y. Soreq, and V. Susic, Model building for flavor changing Higgs couplings, Phys. Rev. D **90**, 115022 (2014).

[40] A. Vicente, Theory and phenomenology of lepton flavor violation, arXiv:1411.2372.

[41] S. M. Boucenna, J. W. F. Valle, and A. Vicente, Predicting charged lepton flavor violation from gauge symmetry, Phys. Rev. D **92**, 053001 (2015).

[42] M. Gomez-Bock and R. Noriega-Papaqui, Flavor violating decays of the Higgs bosons in the THDM-III, J. Phys. G **32**, 761 (2006).

[43] L. de Lima, C. S. Machado, R. D. Matheus, and L. A. F. d. Prado, Higgs flavor violation as a signal to discriminate models, J. High Energy Phys. 11 (2015) 074.

[44] I. Dorsner, S. Fajfer, A. Greljo, J. F. Kamenik, N. Kosnik, and I. Nisandzic, New physics models facing lepton flavor violating Higgs decays at the percent level, J. High Energy Phys. 06 (2015) 108.

[45] Y. Omura, E. Senaha, and K. Tobe, Lepton-flavor-violating Higgs decay $h \to \mu\tau$ and muon anomalous magnetic moment in a general two Higgs doublet model, J. High Energy Phys. 05 (2015) 028.

[46] G. Cvetic, S. S. Hwang, and C. S. Kim, One loop renormalization group equations of the general framework with two Higgs doublets, Int. J. Mod. Phys. A **14**, 769 (1999).

[47] G. Cvetic, S. S. Hwang, and C. S. Kim, Higgs mediated flavor changing neutral currents in the general framework with two Higgs doublets: An RGE analysis, Phys. Rev. D **58**, 116003 (1998).

[48] A. Fernandez, C. Pagliarone, F. Ramirez-Zavaleta, and J. J. Toscano, Higgs mediated double flavor violating top decays in effective theories, J. Phys. G **37**, 085007 (2010).

[49] U. Cotti, L. Diaz-Cruz, C. Pagliarone, and E. Vataga, Search for the Lepton Flavour Violating Higgs decay $H \to \tau\mu$ at Hadron Colliders, eConf **C010630**, P102 (2001).

[50] S. Bar-Shalom, A. Rajaraman, D. Whiteson, and F. Yu, Collider signals of maximal flavor violation: Same-sign leptons from same-sign tops at the Tevatron, Phys. Rev. D **78**, 033003 (2008).

[51] F. Larios, R. Martinez, and M. A. Perez, Constraints on top quark FCNC from electroweak precision measurements, Phys. Rev. D **72**, 057504 (2005).

[52] K. A. Assamagan, A. Deandrea, and P. A. Delsart, Search for the lepton flavor violating decay $A^0/H^0 \to \tau^{\pm}\mu^{\mp}$ at hadron colliders, Phys. Rev. D **67**, 035001 (2003).

[53] T. Han and D. Marfatia, $h \to \mu\tau$ at Hadron Colliders, Phys. Rev. Lett. **86**, 1442 (2001).

[54] N. Craig and S. Thomas, Exclusive signals of an extended Higgs sector, J. High Energy Phys. 11 (2012) 083.

[55] N. Craig, J. Galloway, and S. Thomas, Searching for Signs of the Second Higgs Doublet, arXiv:1305.2424.

[56] B. Dumont, J. F. Gunion, Y. Jiang, and S. Kraml, Constraints on and future prospects for two-Higgs-doublet models in light of the LHC Higgs signal, Phys. Rev. D **90**, 035021 (2014).

[57] E. Brownson, N. Craig, U. Heintz, G. Kukartsev, M. Narain, N. Parashar, and J. Stupak, Heavy Higgs Scalars at Future Hadron Colliders (A Snowmass Whitepaper), arXiv:1308.6334.

[58] B. Coleppa, F. Kling, and S. Su, Constraining type II 2HDM in light of LHC Higgs searches, J. High Energy Phys. 01 (2014) 161.

[59] B. Holdom and M. Ratzlaff, Distinctive heavy Higgs decays, Phys. Rev. D **91**, 035031 (2015).

[60] ATLAS Collaboration, Report No. ATLAS-CONF-2013-027.

[61] V. Khachatryan *et al.* (CMS Collaboration), Search for lepton-flavour-violating decays of the Higgs boson, Phys. Lett. B **749**, 337 (2015).

[62] A. R. Johansen and M. Sher, The electron/muon specific two Higgs doublet model at e + e− colliders, Phys. Rev. D **91**, 054021 (2015).

[63] https://lhec.web.cern.ch.

[64] See for e. g., M. Klein and R. Yoshida, Collider Physics at HERA, Prog. Part. Nucl. Phys. **61**, 343 (2008).

[65] I. A. Sarmiento-Alvarado, A. O. Bouzas, and F. Larios, Analysis of the top-quark charged-current coupling at the LHeC, J. Phys. G **42**, 085001 (2015).

[66] H. Baer *et al.*, The International Linear Collider Technical Design Report - Volume 2: Physics, arXiv:1306.6352.

[67] K. A. Olive *et al.* (Particle Data Group Collaboration), Review of particle physics, Chin. Phys. C **38**, 090001 (2014).

[68] S. L. Glashow and S. Weinberg, Natural conservation laws for neutral currents, Phys. Rev. D **15**, 1958 (1977); E. A. Paschos, Diagonal neutral currents, Phys. Rev. D **15**, 1966 (1977).

[69] T. P. Cheng and M. Sher, Mass matrix ansatz and flavor nonconservation in models with multiple Higgs doublets, Phys. Rev. D **35**, 3484 (1987).

[70] J. Hernandez-Sanchez, L. Lopez-Lozano, R. Noriega-Papaqui, and A. Rosado, Couplings of quarks in the partially aligned 2HDM with a four-zero texture Yukawa matrix, Phys. Rev. D **85**, 071301 (2012).

[71] H. Fritzsch and Z. z. Xing, Four zero texture of Hermitian quark mass matrices and current experimental tests, Phys. Lett. B **555**, 63 (2003).

[72] Y. Grossman, Phenomenology of models with more than two Higgs doublets, Nucl. Phys. **B426**, 355 (1994).

[73] A. G. Akeroyd, S. Moretti, and J. Hernandez-Sanchez, Light charged Higgs bosons decaying to charm and bottom quarks in models with two or more Higgs doublets, Phys. Rev. D **85**, 115002 (2012).

[74] M. Aoki, S. Kanemura, K. Tsumura, and K. Yagyu, Models of Yukawa interaction in the two Higgs doublet model, and their collider phenomenology, Phys. Rev. D **80**, 015017 (2009).

[75] I. F. Ginzburg and I. P. Ivanov, Tree-level unitarity constraints in the most general 2HDM, Phys. Rev. D **72**, 115010 (2005).

[76] A. Crivellin, C. Greub, and A. Kokulu, Flavor-phenomenology of two-Higgs-doublet models with generic Yukawa structure, Phys. Rev. D **87**, 094031 (2013).

[77] O. Deschamps, S. Monteil, V. Niess, S. Descotes-Genon, S. T'Jampens, and V. Tisserand, The two Higgs doublet of type II facing flavour physics data, Phys. Rev. D **82**, 073012 (2010).

[78] S. Kanemura, M. Kikuchi, and K. Yagyu, Fingerprinting the extended Higgs sector using one-loop corrected Higgs boson couplings and future precision measurements, Nucl. Phys. **B896**, 80 (2015).

[79] A. Biswas and A. Lahiri, Masses of physical scalars in two Higgs doublet models, Phys. Rev. D **91**, 115012 (2015).

[80] D. Das, New limits on $\tan\beta$ for 2HDMs with $\mathbf{Z_2}$ symmetry, Int. J. Mod. Phys. A **30**, 1550158 (2015).

[81] A. Belyaev, N. D. Christensen, and A. Pukhov, CalcHEP 3.4 for collider physics within and beyond the

standard model, Comput. Phys. Commun. **184**, 1729 (2013).
[82] O. Bruening and M. Klein, The Large Hadron Electron Collider, Mod. Phys. Lett. A **28**, 1330011 (2013).
[83] J. L. Abelleira Fernandez *et al.* (LHeC Study Group Collaboration), On the Relation of the LHeC and the LHC, arXiv:1211.5102.
[84] J. L. Abelleira Fernandez *et al.* (LHeC Study Group Collaboration), A Large Hadron Electron Collider at CERN: Report on the physics and design concepts for machine and detector, J. Phys. G **39**, 075001 (2012).
[85] Bruce Mellado (LHeC Study Group Collaboration), Topics in the Relation of the LHeC and the LHC, J. Phys. Conf. Ser. **455**, 012019 (2013).
[86] See for e. g. R. B. Appleby, L. Thompson, B. Holzer, M. Fitterer, N. Bernard, and P. Kostka, The high luminosity interaction region for a ring-ring Large Hadron Electron Collider, J. Phys. G **40**, 125004 (2013).
[87] J. Pumplin, D. R. Stump, J. Huston, H. L. Lai, P. M. Nadolsky, and W. K. Tung, New generation of parton distributions with uncertainties from global QCD analysis, J. High Energy Phys. 07 (2002) 012.
[88] T. Sjostrand, S. Mrenna, and P. Z. Skands, PYTHIA 6.4 physics and manual, J. High Energy Phys. 05 (2006) 026.
[89] J. R. Ellis, M. K. Gaillard, and D. V. Nanopoulos, A phenomenological profile of the Higgs boson, Nucl. Phys. **B106**, 292 (1976).
[90] J. M. LoSecco, Higgs boson production in neutrino scattering, Phys. Rev. D **14**, 1352 (1976).
[91] R. M. Godbole, Trimuon events due to neutrino and antineutrino induced production of vector mesons and Higgs boson, Phys. Rev. D **18**, 95 (1978).
[92] Z. Hioki, S. Midorikawa, and H. Nishiura, Higgs boson production in high-energy lepton—nucleon scattering, Prog. Theor. Phys. **69**, 1484 (1983).
[93] T. Han and H. C. Liu, Production of charged and neutral Higgs bosons in high-energy lepton nucleon interactions, Z. Phys. C **28**, 295 (1985).
[94] J. Blumlein, G. J. van Oldenborgh, and R. Ruckl, QCD and QED corrections to Higgs boson production in charged current e p scattering, Nucl. Phys. **B395**, 35 (1993).
[95] R. Kleiss and W. J. Stirling, Tagging the Higgs, Phys. Lett. B **200**, 193 (1988).
[96] V. D. Barger, T. Han, and R. J. N. Phillips, Improving the heavy Higgs boson two charged lepton—two neutrino signal, Phys. Rev. D **37**, 2005 (1988).
[97] V. Barger, K. Cheung, T. Han, and R. J. N. Phillips, Strong W^+W^+ scattering signals at pp supercolliders, Phys. Rev. D **42**, 3052 (1990).
[98] T. Han and B. Mellado, Higgs Boson Searches and the H b anti-b Coupling at the LHeC, Phys. Rev. D **82**, 016009 (2010).
[99] Z. Wen, S. M. Wang, W. G. Ma, L. Guo, and R. Y. Zhang, The light MSSM neutral Higgs boson production associated with an electron and a jet at the LHeC, Phys. Rev. D **83**, 055003 (2011).
[100] S. P. Das and M. Drees, *CP*-violating supersymmetric Higgs at the Tevatron and LHC, Phys. Rev. D **83**, 035003 (2011).
[101] S. P. Das and M. Drees, *CP*-violating MSSM Higgs at Tevatron and LHC, J. Phys. Conf. Ser. **259**, 012071 (2010).
[102] S. P. Das, A. Datta, and M. Drees, *CP*-violating Higgs at Tevatron, AIP Conf. Proc. **1078**, 223 (2009).